MECHANICAL BEHAVIOR AND LEACHING CHARACTERISTICS OF SILICOMANGANESE-FUME INCORPORATED CEMENTITIOUS COMPOSITES

BY

SHAYIQ RASHID

A Thesis Presented to the

COLLEGE OF GRADUATE AND INTERDISCIPLINARY STUDIES

KING FAHD UNIVERSITY OF PETROLEUM & MINERALS

DHAHRAN, SAUDI ARABIA

In Partial Fulfillment of the
Requirements for the Degree of

MASTER OF SCIENCE

In

CIVIL AND ENVIRONMENTAL ENGINEERING

DECEMBER, 2024

KING FAHD UNIVERSITY OF PETROLEUM & MINERALS

DHAHRAN- 31261, SAUDI ARABIA

DEANSHIP OF GRADUATE STUDIES

This thesis, written by **SHAYIQ RASHID** under the direction of his thesis advisor and approved by his thesis committee, has been presented and accepted by the Dean of Graduate Studies in partial fulfillment of the requirements for the degree of **MASTER OF SCIENCE IN CIVIL ENGINEERING**.

Dr. Asad Hanif
(Advisor)

Prof. Shamsad Ahmad
Department Chairman

Dr. Hammad Raza Khalid
(Co-Advisor)

Dr. Suliman Al-Homidan
Dean of Graduate Studies

Prof. Hong S. Wong
(External Member)

Date

Dr. Abbas Ahmed Albu Shaqraa
(Member)

COLLEGE OF GRADUATE AND INTERDISCIPLINARY STUDIES

Dr. Saheed Adekunle
(Member)

I dedicate this work to my parents, sister and other family members especially my grandparents

ACKNOWLEDGMENTS

In the name of Allah (S.W.T), the Most Gracious, the Most Merciful. All praise and thanks are due to Almighty Allah, whose mercy and guidance have helped me complete this thesis. Without His blessings, this journey would not have been possible. Alhamdulillah. I extend my heartfelt gratitude to King Fahd University of Petroleum and Minerals (KFUPM) for providing me with the platform, financial support, and resources necessary to pursue my research. The institution's commitment to academic excellence and research has contributed significantly to the success of this work.

I am deeply grateful to my advisor, Dr. Asad Hanif, and co-advisor, Dr. Hammad Raza Khalid, for their invaluable guidance, support, and encouragement. Their expertise and mentorship have significantly enriched my research. I appreciate my thesis committee members, Dr. Hong S. Wong, Dr. Abbas Ahmed Albu Shaqraa, and Dr. Saheed Adekunle, for their insightful feedback and unwavering support.

I would like to express my gratitude to lab engineer Er. Tariq, Er. Najamuddin, and Er. Khalid for their technical assistance and dedication, which ensured the smooth execution of my experiments.

Finally, I sincerely thank my family and friends for their continuous support, encouragement, and prayers. Their belief in me and their unwavering support has been a source of strength and motivation.

I pray that Allah continues to bless us all with knowledge, wisdom, and the ability to contribute positively to society. May He accept this humble effort and grant us success in all our endeavors. Ameen

TABLE OF CONTENTS

LIST OF TABLES

LIST OF FIGURES

LIST OF ABBREVIATIONS

SCM	:	Supplementary Cementitious Materials
SMF	:	Silicomanganese Fume
OPC	:	Ordinary Portland Cement
C-S-H	:	Calcium Silicate Hydrate
CH	:	Calcium Hydroxide/ Portlandite
C_3S	:	Tricalcium silicate/Alite
C_2S	:	Dicalcium silicate/Belite
C_3A	:	Tricalcium Aluminate
C_4AF	:	Tetracalcium Aluminoferrite

ABSTRACT

Full Name : SHAYIQ RASHID

Thesis Title : MECHANICAL BEHAVIOR AND MANGANESE LEACHING CHARACTERISTICS OF SILICOMANGANESE FUME INCORPORATED GREEN CEMENTITIOUS COMPOSITES

Major Field : CIVIL ENGINEERING

Date of Degree : December, 2024

This study investigates the feasibility of incorporating silicomanganese fume (SMF) into concrete by replacing varying percentages of cement with SMF (0%, 10%, 20%, and 30%). The reactivity of different grades of SMF (SMF1, SMF2, and SMF3) was evaluated using isothermal calorimetry by replacing 20% of OPC with SMFs and their effect on fresh, mechanical, and microstructural properties. The mechanical properties, hydration behavior, and microstructural characteristics were thoroughly investigated. The results demonstrated an 8% increase in compressive strength with up to 20% cement replacement by SMF compared to the control specimen. However, beyond the 20% replacement level, the impact was negative. Further, the leaching behavior of manganese (Mn, a hazardous element) and Calcium (Ca) was evaluated using ICP-OES analysis. Minimal Mn leaching was observed in the first two days, with a maximum leaching of about 0.002 mg/L in the specimen with 30% SMF, and no leaching of Mn was detected after 2 days. Ca leaching was detected, and about 50% less Ca ions were present in the specimens subjected to leaching compared to specimens not subjected to leaching. The Control(C) specimen showed maximum Ca leaching at 90 days, with about 234 mg/L. Microstructural investigations by SEM/EDX, XRD, and TGA further confirmed that SMF is a cement substitute, enhancing microstructure when used within specified limits. The portlandite

content and amount of chemically bound water validated the increased degree of hydration. The resulting denser and more compact microstructure with lower porosity substantiated the results of mechanical properties and Mn leaching.

ملخص الرسالة

الاسم الكامل: شايق رشيد

عنوان الرسالة: سلوك المواد الميكانيكية وخصائص تسريب المانجانيز لمركبات الأسمنت الأخضر المدمجة بدخان السيليكو مانجانيز

التخصص: الهندسة المدنية

تاريخ الدرجة العلمية: ديسمبر 2024

في هذه الدراسة، يتم التحقيق في جدوى دمج الدخان السيليكوني (SMF) في الخرسانة عن طريق استبدال نسب متفاوتة من الأسمنت ب SMF (0٪ و 10٪ و 20٪ و 30٪). تمت دراسة الخصائص الميكانيكية الناتجة وسمات الترطيب والخصائص المجهرية بالتفصيل. أظهرت النتائج تأثيرا إيجابيا على قوة الضغط لاستبدال الأسمنت بنسبة تصل إلى 20٪ بواسطة SMF، مما أدى إلى زيادة بنسبة 8٪ مقارنة بعينة التحكم. ومع ذلك، بالإضافة إلى مستوى الاستبدال بنسبة 20٪، كان التأثير سلبيا. علاوة على ذلك، تم تقييم سلوك ترشيح المنغنيز (Mn، وهو عنصر خطير) والكالسيوم (Ca) باستخدام تحليل ICP-OES. لوحظ الحد الأدنى من الرشح Mn في اليومين الأولين، مع الحد الأقصى للرشح حوالي 0.002 ملغم / لتر في العينة مع 30٪ SMF، ولم يتم اكتشاف أي رشح من Mn بعد يومين. تم اكتشاف رشح Ca، وكان هناك حوالي 50٪ أقل من أيونات Ca في العينات المعرضة للرشح مقارنة بالعينات التي لم تخضع للرشح. أظهرت عينة التحكم (C) الحد الأقصى لرشح Ca في 90 يوما، مع حوالي 234 ملغم / لتر. أكدت تحقيقات البنية المجهرية التي أجراها SEM/EDX وXRD وTGA كذلك أن SMF هو بديل للأسمنت، مما يعزز البنية المجهرية عند استخدامه ضمن حدود محددة. تحقق محتوى بورتلانديت وكمية المياه المرتبطة كيميائيا من زيادة درجة الترطيب. أثبرت البنية المجهرية الأكثر كثافة والأكثر إحكاما مع مسامية أقل نتائج الخواص الميكانيكية ورشح Mn. علاوة على ذلك، تم تقييم تفاعل درجات مختلفة من SMF (SMF1 وSMF2 وSMF3) باستخدام قياس السعرات الحرارية متساوي الحرارة عن طريق استبدال 20٪ من OPC بواسطة SMFs وتأثيرها على الخصائص الجديدة والميكانيكية والبنية المجهرية.

CHAPTER 1

INTRODUCTION

The construction industry plays a significant role in global carbon dioxide (CO_2) emissions, with cement production alone accounting for about 8% of the world's total CO_2 emissions[1]. Cement, the key ingredient in concrete, is produced through an energy-intensive process that involves heating limestone (calcium carbonate) to produce clinker. This process releases significant CO_2 from decomposing calcium carbonate and burning fossil fuels in cement kilns. With the growing demand for construction worldwide, especially in rapidly developing regions, the environmental impact of cement production has faced heightened scrutiny. Minimizing the carbon footprint of construction materials has thus become a critical focus in mitigating climate change.

One promising approach to lowering emissions in the construction sector is partially replacing Portland cement with Supplementary Cementitious Materials (SCMs). These materials, when blended with cement, enhance the properties of cementitious composites by contributing to the hydration or acting as a filler. Common SCMs include industrial byproducts such as fly ash, ground granulated blast furnace slag (GGBFS), and silicomanganese fume from coal-fired power plants, steel production, and silicon alloy manufacturing, respectively[2–4]. These materials offer a dual advantage: they enhance the durability and mechanical properties of resulting concrete while reducing the amount of Portland cement required. This lessens CO_2 emissions linked with the production of cement and promotes the sustainable reuse of industrial waste that would otherwise be landfilled.

SCMs enhance concrete performance through their pozzolanic and latent hydraulic reactions, which generate additional calcium silicate hydrates (CSH) when combined with water and calcium hydroxide. This additional CSH strengthens the concrete matrix, reducing porosity and increasing resistance to various forms of deterioration, such as chemical attacks, sulfate exposure, and alkali-silica reactions. For example, fly ash and GGBS enhance the workability of fresh concrete while providing long-term strength gains and improved resistance to cracking. Silica fume, with its extremely fine particles, significantly increases the density and impermeability of concrete, which is particularly beneficial in aggressive environments. By improving the durability of concrete, SCMs reduce the frequency of repairs and maintenance, thereby lowering the long-term environmental and economic costs of infrastructure projects.

Among the various SCMs, silicomanganese fume (SMF), a byproduct of silicomanganese alloy production, has emerged as a valuable additive for cementitious materials. SMF is generated during the smelting process of silicomanganese, an essential alloy used in steel production and contains high concentrations of silica (SiO_2) and manganese oxides (MnO). These components impart SMF with pozzolanic properties, allowing it to react with portlandite in the cement matrix to form secondary C-S-H. Incorporating SMF in between 10% to 20% concrete mixes has been found to improve mechanical properties [5,6].

This thesis aims to comprehensively explore the leaching behavior of manganese and calcium in SMF-incorporated concrete, its effects on the mechanical and microstructural properties of SMF-enhanced concrete, and its role in lowering the carbon footprint of construction materials. Through experimental studies, the research will evaluate SMF's potential as a sustainable SCM, contributing to the ongoing effort to develop more eco-friendly and durable construction practices.

1.1 Research Gap

A few studies exist on the use of Silicomanganese Fume (SMF) as a SCM in the making of SCC(Self-compacting Concrete) [3], used alone or in conjunction with other SCMs such as GGBFS to produce sustainable Alkali-Activated Binders (AABs) and alkaline-activated mortars [4,5]. The SMF has also been incorporated in concrete in different ratios to reduce concrete permeability and increase compressive strength [6]. However, the possible leaching of the hazardous element Mn and Ca and their impact on the mechanical properties of samples remains an unexplored field of research. This knowledge gap highlights the necessity of examining Mn and Ca leaching in SMF-incorporated cement concrete to assure environmental safety and material integrity. There is also a need for more research on different grades of SMF's reactivity and their impact on the microstructural and mechanical properties of SMF-incorporated cement pastes.

This study explores the leaching behavior of Mn and Ca using paste specimens incorporating SMF. The state-of-the-art technique of inductively coupled plasma optical emission spectrometry (ICP-OES) was employed to quantify and analyze Mn and ca leaching. The leaching characteristics of Mn and Ca were studied for 90 days at various intervals [7]. Moreover, the influence of multiple ratios of SMF on the microstructural properties and strength of concrete was explored. These analyses were done before and after the leaching process to investigate the change in microstructure leading to a possible increase or decrease in strength with various proportions of SMF. Compressive strength is a critical factor for structural integrity, and SMF incorporation may contribute positively to this property. The compressive strength of SMF-incorporated paste specimens was determined and compared to the control specimens. In addition, SEM (Scanning electron Microscopy), XRD (X-ray Diffractometry), and TGA/DTG (Thermogravimetry/Differential Thermogravimetry) analyses were used to observe the microstructural changes within the matrix, which helped with comprehending the distribution and morphology of hydration products, mineral compositions, and the quantification of Portlandite and non-evaporable water.

The outcomes of this investigation are expected to yield significant insights into optimizing concrete mix designs for enhanced durability and environmental safety, contributing to the broader field of sustainable construction materials.

1.2 Research Significance

This research is significant because it has the potential to address critical challenges in sustainable construction materials by exploring the innovative use of SMF to enhance mechanical properties, ensure environmental safety, and reduce carbon footprints. The following points highlight the significance of this study.

- Understanding the leaching extent of Mn and Ca from SMF-incorporated concrete is essential to assess its environmental impact.
- Mn leaching can contaminate soil, groundwater, and nearby ecosystems and may lead to health issues.
- Mn and Ca leaching may affect concrete durability and long-term performance, affecting the material integrity and reducing service life.

- Reactivity of different grades of SMF will give us a better understanding of its performance in the concrete.

1.3 Research Objectives

The primary objective of this research is to explore the Suitability of incorporating Silicomanganese Fume (SMF) in cement paste. The specific objectives are outlined below.

1. Explore the possible leaching of manganese from SMF-incorporated cement paste samples over time.
2. Study the influence of different grades of SMF on the reactivity and mechanical properties of cement paste samples.
3. Examine the impact of varying proportions of SMF on the durability and mechanical strength of cement paste samples.
4. Evaluate the correlation between the leaching behavior and the microstructural properties of the SMF-incorporated samples, both in scenarios with and without the occurrence of leaching.
5. Carry out the cost-benefit analysis to ascertain the usefulness and applicability of SMF.

CHAPTER 2

LITERATURE REVIEW

Global warming, the alarming increase in Earth's average surface temperature, is predominantly caused by anthropogenic actions that emit greenhouse gases, such as carbon dioxide (CO_2), nitrous oxide (N_2O), and methane (CH_4). These gases amplify the greenhouse effect by capturing heat in the atmosphere and increasing temperatures. Since the industrial era, the combustion of fossil fuels, deforestation, and industrial processes have substantially increased atmospheric CO_2 levels, accelerating global temperature rise[8–10]. In 1850, atmospheric CO_2 concentrations increased significantly from 285 ppm to 410 ppm in 2019. As per Global Monitoring Laboratory, the amount of CO_2 rose from 365 ppm in 2002 to 422 ppm as of Sep-2024[11]. There is broad agreement among scientists that human-induced climate change is causing profound impacts on the environment and human societies[12].

2.1 Carbon dioxide production due to the concrete industry

The foundation of the concrete industry is cement as a binder. Approximately four billion tons of cement are produced worldwide annually [13]. The current trends indicate that by the end of this decade, this figure is expected to surpass current levels, and by the year 2050, the demand for concrete is expected to go beyond 18 billion tons per year [14,15]. Concurrently, the manufacturing process of OPC (Ordinary Portland Cement) inherently generates an equal amount of CO_2, with each ton of OPC manufactured generating one ton of CO_2 [13,16,17], which is the primary anthropogenic cause of greenhouse gases [18–20]. Figure 1 shows the typical manufacturing process of dry cement. Cement production is extremely energy-demanding, accounting for about 12 to 15% of the energy consumed by industries [21]. Cement production can broadly be categorized into three phases. The raw meal is prepared in the first stage by crushing, blending, and grounding raw materials like limestone and clay. In the subsequent stage, the prepared raw meal is heated in a cement kiln at around 1400 ºC to 1500 ºC to produce clinker. Finally, the clinker is cooled and ground with Gypsum/anhydrite and supplementary cementitious materials. This ground powder (cement) is finally packed and transported. The CO_2 associated with the cement manufacturing process is mainly due to the calcination of raw limestone($CaCO_3$) into lime(CaO) and CO_2 during the clinker, accounting for about 50% of CO_2 emissions by the cement manufacturing industry [22,23]. Fossil fuels account for about 40% of the total, and the rest is due to electric appliances and transportation [24].

$$CaCO_3 \rightarrow CaO + CO_2 \tag{1}$$

About 1.6 billion metric tonnes of CO_2 was emitted by the cement industry alone in 2022, which has exponentially increased since 1960, as shown in Figure 2, accounting for about 8% of total CO_2 produced worldwide. The countries with the highest CO2 emissions include China, Europe, India, and the United States[25]. The cement industries in the KSA produced about 30 million tonnes of CO_2 in 2022 [26].

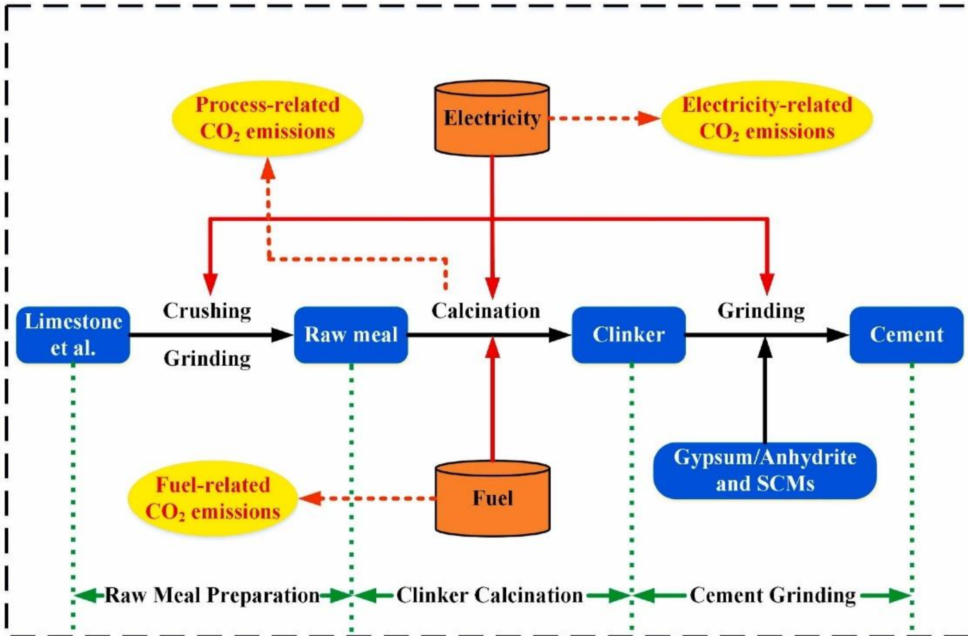

Figure 1 Flow diagram of cement production [2]

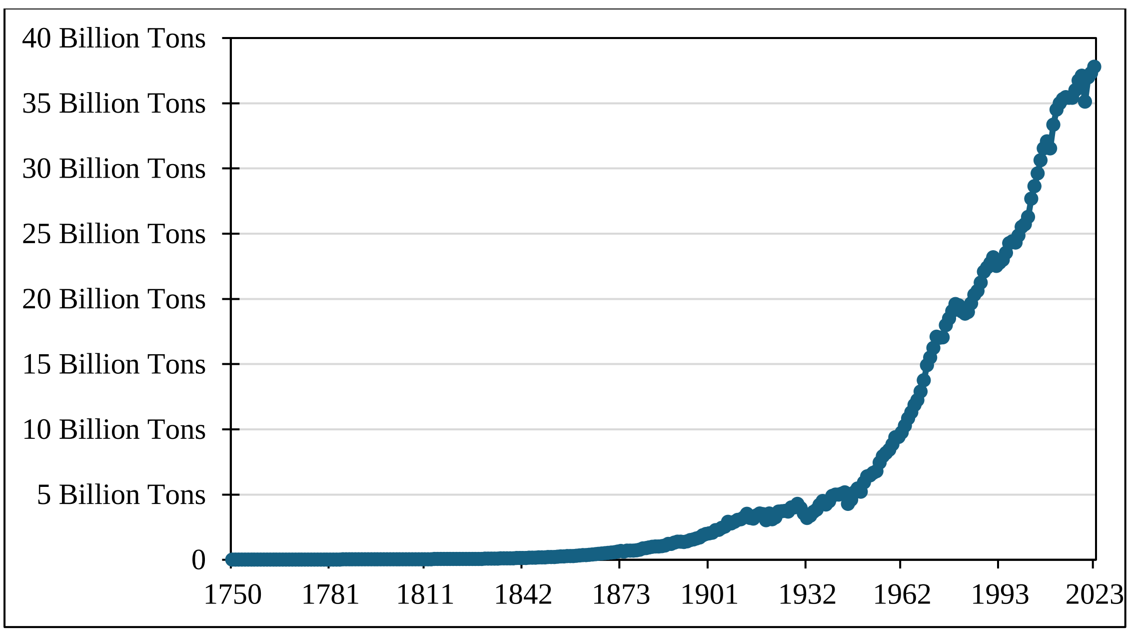

Figure 2 Global CO_2 emissions from 1750 to 2023 (in billion metric tonnes) [26]**.**

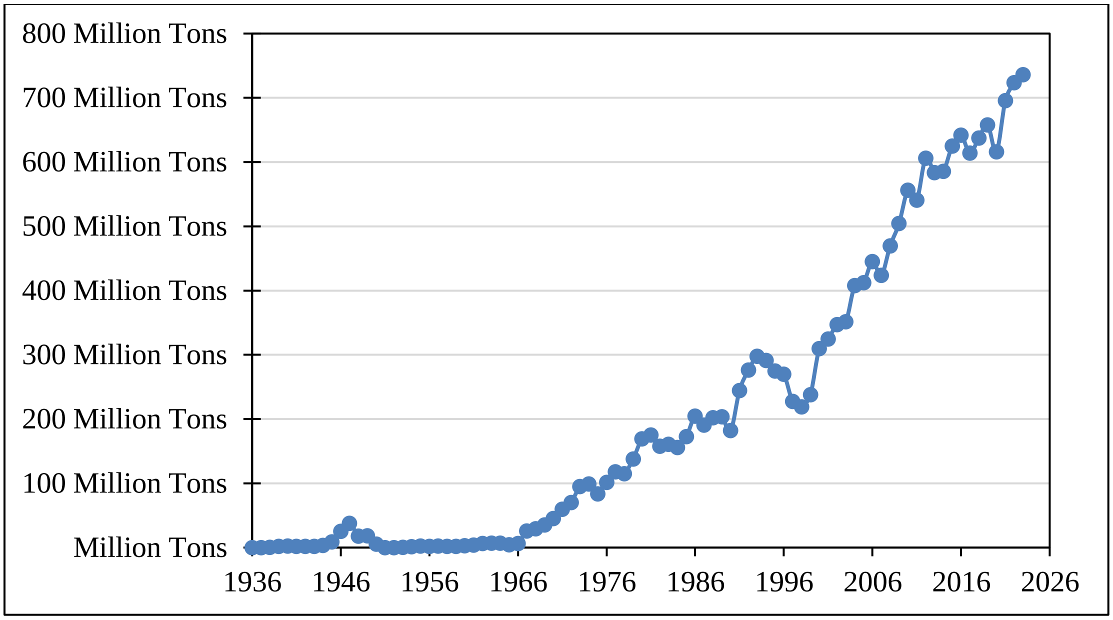

Figure 3 CO_2 emission by the cement industry in Saudi Arabia from 1936 [26].

2.2 Need of Supplementary Cementitious Materials

Engineers and researchers are actively pursuing strategies to curtail cement consumption and its associated CO2 emissions in response to the construction industry's environmental challenges. The Cement Technology Roadmap[27] held in October 2009 suggested four ways to diminish CO_2 emissions from the concrete industry. These include substituting clinker with SCMs, capturing carbon and its storage, using alternative fuels, and improving electric and thermal efficiency. One of the methods explored and suggested is developing and implementing supplementary cementitious materials (SCMs) [28].

SCMs are industrial byproducts or natural materials that can be used as a partial substitution for OPC or as a partial substitution for clinker in cement production [29–31]. Apart from CO_2 emission reductions caused by using SCMs, these also enhance concrete structures' mechanical performance and durability. Various materials are used as SCMs, such as GGBFS, silica fume, fly ash, SMF, steel slag, and biomass ash [31,32]. A significant proportion of the materials currently used as SCMs are byproducts of other industries, such as slag from the steel manufacturing sector and fly ash from coal-fired power plants [33]. Natural materials need less energy input in processing than OPC. For instance, OPC has 3.5 GJ/t clinker thermal energy intensity. While making metakaolin SCM by calcination has only 0.35GJ/t clay [27,31], this accounts for only about 10% of OPC.

SCMs are categorized as inert fillers or reactive SCMs. The latter can be either hydraulic or pozzolanic, and the former doesn't show either of the two but shows filler effects [34]. Hydraulic materials can react with water to produce cementitious compounds independently of calcium hydroxide. GGBFS and calcined clay fall under this category. Pozzolanic materials do not have cementitious properties but react with portlandite to form additional cementitious compounds. Silica fume, natural pozzolans, and fly ash fall under this category. Some materials lie in between but are not entirely inert as their reaction with aluminate or other SCMs leads to the formation of phases of carbo aluminates [35–37]. Studies have shown that higher clinker replacement levels of inert fillers, usually greater than 20%, negatively affect durability and performance. On the other hand, SCMs show positive effects even at higher clinker replacements as these react chemically with portlandite, forming hydration products. Amorphous phases like silica are usually reactive components of SCMs. However, there are exceptions like Zeolites or phases of calcium-rich steel slags [13,38]. Hence it can be generalised that the materials containing amorphous phases in large amounts can be considered as the ideal SCM. However, we cannot use them directly in concrete or cement unless they meet the required chemical and physical properties, reactivity, and adequate supply is available. Furthermore, it should not negatively affect the environment, hydration, consistency, or strength development. The fly ash production chain faces a significant threat, as the United States has already closed 40% of its coal-based power plants. Similarly, the United Kingdom intends to shut down all coal-based power plants by 2025, and the Netherlands intends to do so by 2030 [39]. This leads to the exploration of alternative sources of SCMs and demand testing their quality and their effect on properties like reactivity, mechanical, and leaching characteristics of the concrete. One of the promising alternatives (SCM) is Silicomanganese Fume, and such alternatives are likely to compensate for the higher demand for SCMs in the near future.

2.3 Silicomanganese Fume as Supplementary Cementitious material

SMF is a manganese-rich byproduct of the steel industry. It is generated during ferroalloy production, which is primarily used as a deoxidizing agent in the steel industry. Manganese (Mn) plays a crucial role in steelmaking, where it removes sulfur and oxygen during the conversion of iron ore to steel[40]. The steel industry uses almost 93% of the Mn produced worldwide[41]. In 2020, the worldwide silicomanganese alloy production reached about 16 million tons[42]. According to recent reports, a metric ton of Mn alloy produced, approximately 0.1 metric tonnes of SMF is generated[43,44]. This equates to an annual global production of approximately 1.6 million tons of SMF.

Recently, SMF has gained attention for its pozzolanic properties and ultrafine particle size (ranging from micro to nanoscale), making it a potential supplementary cementitious material (SCM) [45–47]. The dominant oxides present in the SMF are SiO_2, MnO, and K_2O, with 14.5%, 33.1%, and 27.2%, respectively [48]. 70% of SMF is made of Si, Mn, and K [49], as determined from the elemental analysis [50]. Beyond its use in cement, SMF is employed in road construction and drilling fluids[44,51,52]. However, studies exploring its potential remain limited.

Nasir et al.[47] Investigated the magnesium sulfate ($MgSO_4$) exposure of alkali-activated SMF-based cementitious composites, concentrating on varying the concentrations of ground blast furnace slag (GBFS) and alkaline activator content and their effect on mechanical properties and microstructure. The results indicate that specimens with higher GBFS content (30%) and elevated alkali concentrations exhibit significantly better performance, retaining residual compressive strengths of 29.4 to 39.1 MPa after 40 weeks of exposure to $MgSO_4$, resulting in about 60.1% strength retention. In contrast, milder alkali systems showed lower strengths (14.2 to 28.6 MPa) and only 36.5% strength retention. The study highlights that optimal GBFS and alkali activator proportions enhance the formation of a dense microstructural matrix, effectively mitigating damage from sulfate ion diffusion and minimizing the formation of harmful expansive compounds like gypsum and brucite. These findings emphasize the potential of SMF-based composites in applications where durability against sulfate attack is critical, suggesting that careful blend design can considerably improve material resilience in aggressive environments.

Another study by Nasir et al. [53] investigated the development of SMF as an AAB(alkali-activated binder) blended with BFS(blast furnace slag), utilizing sodium silicate (Na_2SiO_3) and sodium hydroxide (NaOH) as activators. The effects of different curing methods, including water ponding, heat curing, and ambient curing, were examined, focusing initially on optimizing the oven-curing duration of 3–24 hours at 60 °C, subsequently, temperature optimization was performed in the range of 25–95 °C for a 6-hour curing period. The results demonstrated good synergy among the precursor materials, leading to the formation of critical phases such as C-Mn-S-H, K-A-S-H, and C-(A)-S-H, which contributed to the strength development of the binder. Early compressive strength gains for water and ambient cured specimens reached approximately 50% of their 28-day maximum strengths of 46.4 MPa and 43.5 MPa, respectively. In contrast, oven-cured specimens (at 60 °C for 3 hours) achieved a 3-day strength of 42.6 MPa, with continuous strength improvements observed over 24 hours. A curing duration of 6 hours was deemed optimal from both energy and cost perspectives, yielding 3-, 7-, and 28-day strengths of 38 MPa, 41 MPa, and 45.2 MPa, respectively. The enhanced crystallinity of the C-A-S-H and quartz phases was noted, and the morphology of the specimens indicated a dense and homogeneous structure with fewer unreacted particles, attributed to the formation of stratlingite and gehlenite, which functioned as effective crack fillers and pore blockers.

Nasir et al. [54] and Najamudin et al. [55] provide a comprehensive analysis of the chemical and physical properties of alkali-activated silico-manganese fume, positioning it as an effective supplementary cementitious material (SCM). The study presents a rigorous methodology where varying proportions of SMF were tested in different alkalinity environments to determine their effectiveness in enhancing concrete strength. The chemical composition of SMF, characterized by high silica content (around 30-40%) and the presence of manganese oxides, plays a crucial role in the hydration process when activated with alkalis like sodium hydroxide (NaOH) and sodium silicate (Na_2SiO_3). The research underscores that when SMF is incorporated into AABs, it helps develop a microstructure with a high density of C-S-H gel, significantly enhancing compressive and flexural strengths. The authors conclude that the right proportion of SMF activates the formation of additional binding phases that improve durability against aggressive chemicals commonly found in construction environments. The SMF was also used alone or in conjunction with other SCMs, such as ground granulated blast furnace slag (GGBFS), to produce sustainable Alkali-Activated Binders and alkaline-activated mortars [48,49]

Gawah et al. [6] They investigated the use of silico-manganese fume in the formulation of sustainable self-compacting concrete (SCC). They experimented with several mixtures containing different percentages of SMF (0%, 10%, 20%, and up to 90% replacements of ordinary Portland cement) to assess workability and mechanical properties. The authors compared the flowability using the slump-flow test and conducted compressive strength tests on days 7, 14, 28, and 90. Their findings reveal that including SMF increased the superplasticizer dosage to obtain a particular flow. However, SMF contributes positively to the filling and passing ability of SCC due to its spherical shape and fine particle size, which facilitate more effortless flow under gravitational forces. The SCC with 10% and 20% SMF replacement has shown significant enhancement in mechanical strength. The research highlights that while higher percentages of SMF improve specific properties, they can increase water demand, necessitating careful mixture design. Furthermore, the use of SMF aligns with sustainability goals by reducing the carbon footprint associated with conventional cement production.

Nasir et al. [56] provide a focused investigation into SMF-incorporated composites' strength and microstructural characteristics using a robust statistical approach based on the Taguchi method. They designed a series of experiments that varied four key factors: the content of SMF and silica fume, the sand-to-binder ratio, and the water-to-binder ratio, assessing nine different mortar combinations in the trial mix and then three more mixes for validation of the same data. The results highlighted a striking trend: while the addition of SMF reduced compressive strength compared to pure silica fume mixtures, the synergy observed in blended systems (20% SMF and 5% silica fume) considerably enhanced performance characteristics, achieving compressive strengths of 48.8 MPa. The microstructural analysis using SEM indicated a highly interconnected gel structure in the optimal blend, promoting resistance to crack propagation. This study illustrates that while incorporating SCMs generally influences the mechanical properties, carefully designing mixtures using the Taguchi method can significantly optimize performance outcomes. The SMF has also been incorporated in concrete in different ratios to reduce concrete permeability and increase compressive strength [16].

2.4 Detrimental effects of Mn and Ca leaching from cementitious composites

Mn is an essential element required for various biochemical processes in humans. The absence of it would significantly affect immune function, growth potential, coagulation, biochemical regulations, and removal of byproducts in the human body [57]. However, the higher level of Mn has detrimental effects on humans and the surrounding environment. Many studies have shown that it can lead to adverse health effects when exposed to high levels. These include neurological issues like Manganism [58–60], respiratory problems like manganese pneumonia [61], cognitive and behavioral changes [58], liver damage, cardiovascular issues like hypertension [62], reproductive and developmental effects, gastrointestinal disturbances like abdominal pain [63], vomiting, and diarrhea, impaired immune function, and iron absorption interference. The higher level of Manganese in the soil is also detrimental, as it may mix with groundwater and contaminate it, leading to a decline in crop production and quality and making the groundwater unfit for use [57,64]. High Mn in drinking water sources leads to deficiencies in children and could affect reasoning, IQ scores, memories, and academics [65], entailing comprehensive investigation of incorporating SMF in the concrete. The maximum permissible content of Mn in drinking water is 0.05 mg/L as per the National Research Council, USA and Council of the European Communities. According to the Indian Standard (IS 10500: 2012) and WHO guidelines for drinking water quality, the permissible limit for Mn is 0.1 mg/L [66,67].

Ca leaching from cement paste matrix in concrete structures used for underground members or members constantly subjected to low pH environments like underwater or in concrete structures used to store radioactive waste is of significant concern. Cement-based materials are highly susceptible to decalcification in deionized (pure) water [68–70]. The combined processes of dissolution and diffusion lead to leaching. The concentration gradient created by deionized water leads to the diffusion of Ca ions from the ion-rich pore solution to the surrounding ion-deficient water. This forces the dissolution of CH (calcium hydroxide) and C-S-H (Calcium silicate hydrate) due to the reduction of Ca ions in the pore solution. Consequently, it increases the permeability and affects the mechanical properties of the materials[70].

CHAPTER 3

RESEARCH METHODOLOGY

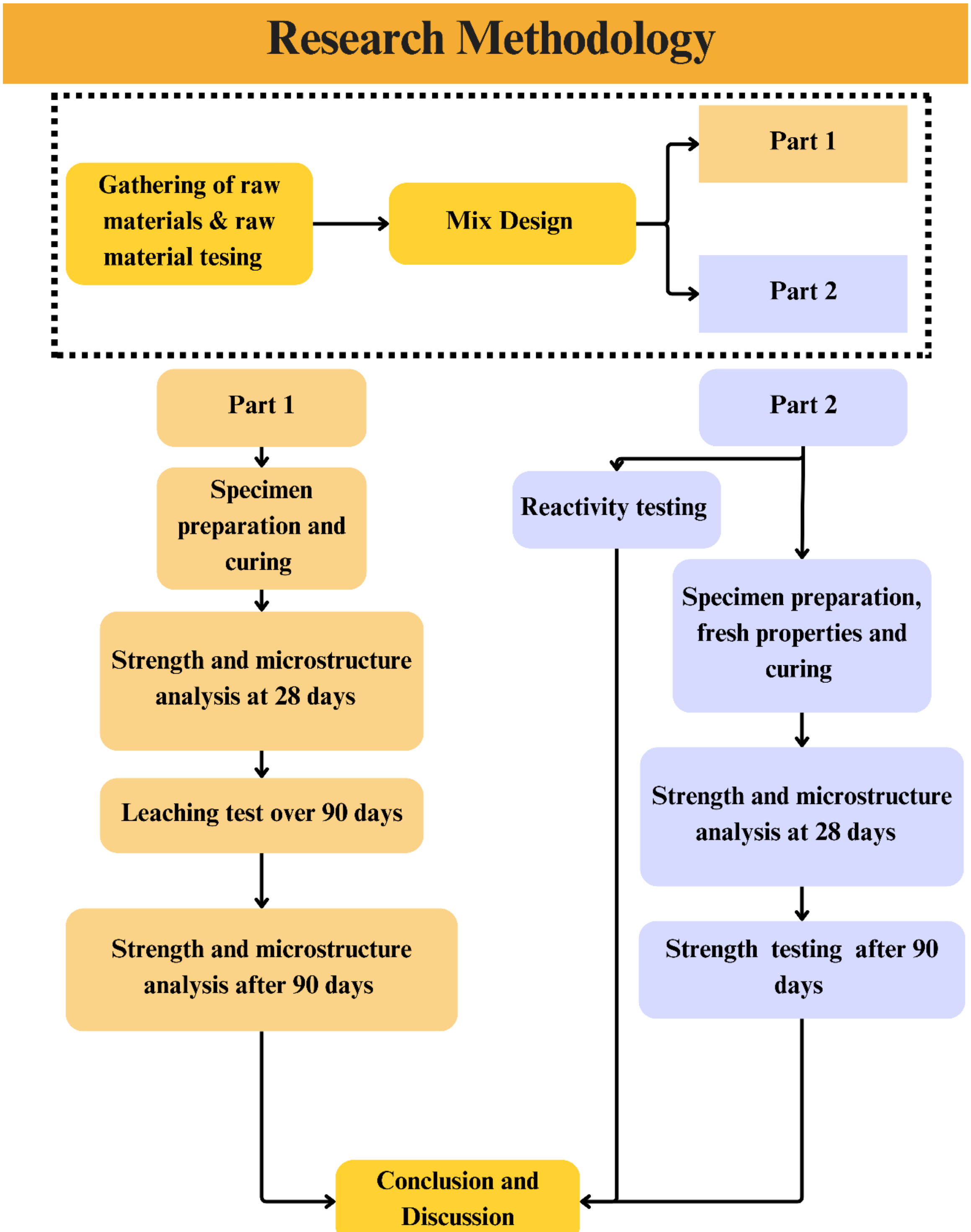

Figure 4 Flow chart of research methodology

3.1 Raw Materials and Mix Design

Based on the findings of the literature survey, the necessary raw materials, including cement, silicomanganese fume (SMF), burlap, polypropylene boxes, and deionized water, were procured. Type I ordinary Portland cement (OPC), as per ASTM C150, possessing a 3.15 specific gravity, was sourced from Saudi Cement. SMF was obtained from the Gulf Ferro Alloy Company (SABAYEK) in Jubail, Saudi Arabia. These materials underwent comprehensive characterization, including chemical composition analysis, microstructural evaluation, and particle size distribution.

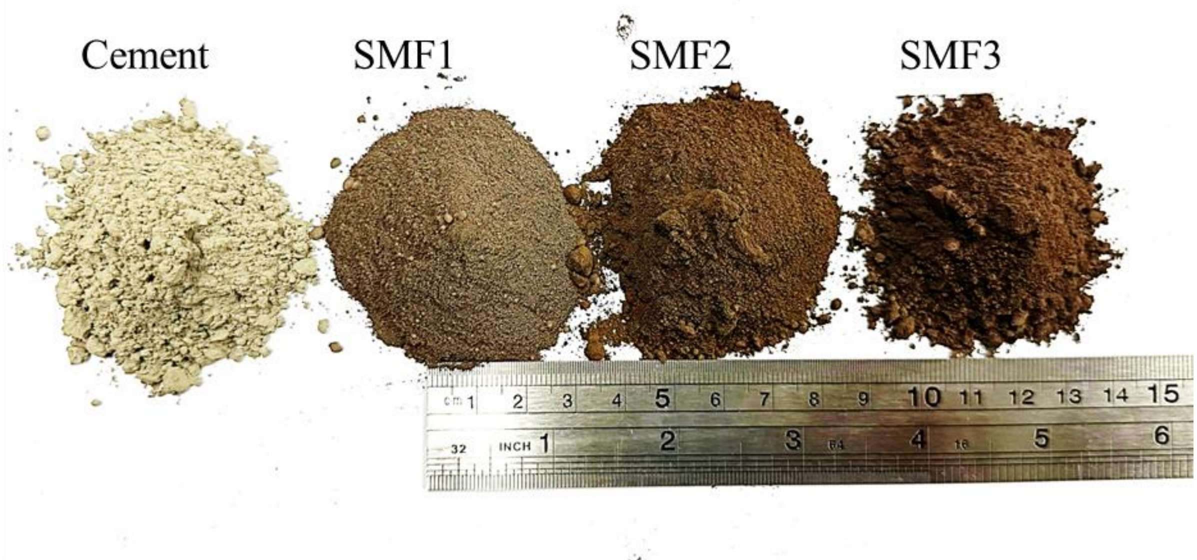

Figure 5 Optical images of raw materials

The particle size distribution of SMF1, SMF2, SMF3, and OPC was determined using an Anton Paar PSA 1190, as shown in Figure 6, yielding mean particle sizes of 3.3764 μm, 0.9836 μm, 8.1804 μm, and 30.3490 μm, respectively. The D10, D50, and D90 particle size metrics are presented in Table 2. The Chemical composition was determined via X-ray fluorescence (XRF) using an M4 TORNADO (BRUKER), with results summarized in Table 1. MnO and SiO2 were identified as the primary components. X-ray diffraction (XRD) analysis, performed on an Ultima IV device (Rigaku), revealed that SMF predominantly contained quartz and manganese ferrite, with minor wollastonite peaks. OPC exhibited major phases of Alite, Belite, C3A, and C4AF, as shown in Figure 7.

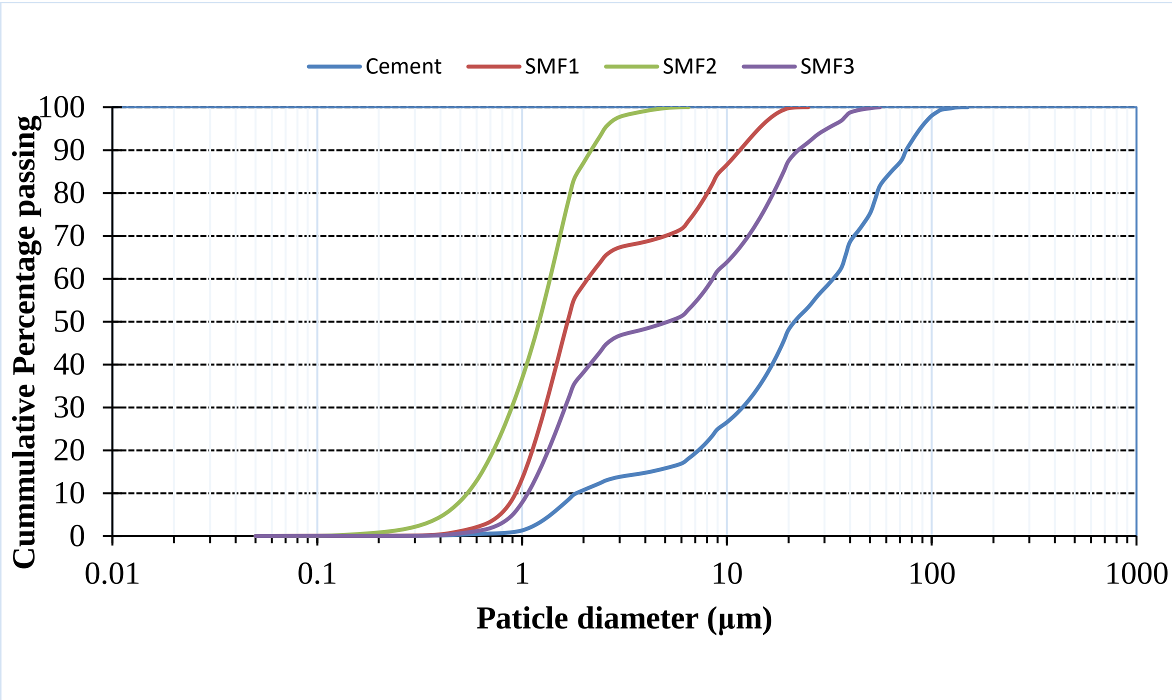

Figure 6 Raw materials particle size distribution

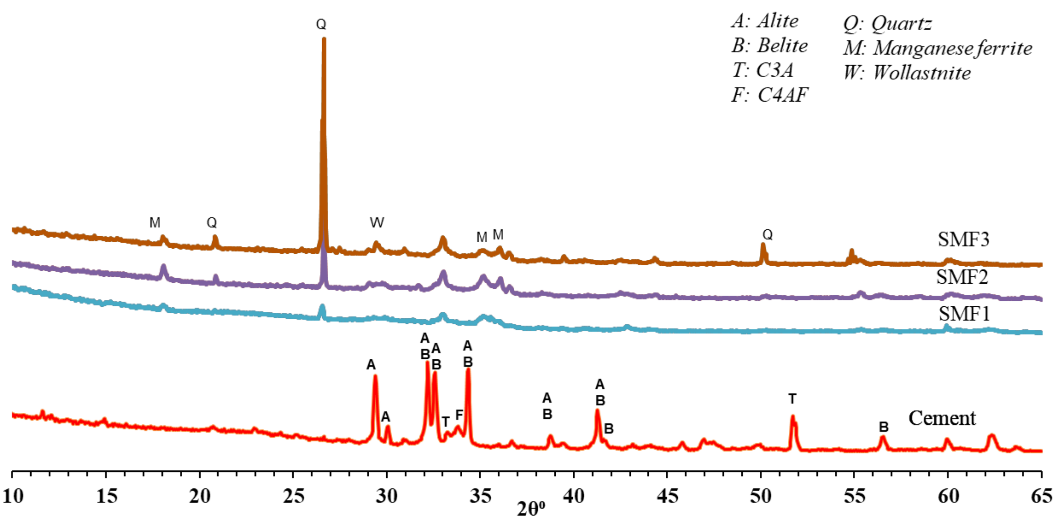

Figure 7 Raw materials XRD

The physical appearance of OPC, SMF1, SMF2, and SMF3 is grey, greyish brown, reddish-brown, and dark brown, respectively, as depicted in Figure 5. The SEM imaging as shown in Figure 8, shows the particle shape as spherical for all SMFs, with greater particle sizes in SMF2 and SMF3 as compared to SMF1. Deionized water was used as a leachate to maintain experimental consistency. Ensuring the quality and uniformity of raw materials was critical for obtaining reliable experimental results. A trial-and-error approach was adopted for mix design optimization, refining material proportions to meet the study's objectives.

Table 1 Chemical composition of raw materials

Chemical composition /Wt %	SiO_2	Fe_2O_3	CaO	MnO	K_2O	SO_3	P_2O_5	Cl	AL_2O_3
Cement	16.27	3.96	73.97	-	-	-	-	-	3.71
SMF1	33.38	3.58	14.79	43.68	2.17	1.06	0.82	0.48	-
SMF2	25.85	7.49	10.77	50.87	2.03	1.49	0.7	0.79	-
SMF3	28.71	5.71	13.43	48.73	1.12	1.04	0.69	0.53	-

Table 2 Particle size data and physical appearance of raw materials

Designation	Physical appearance	D10(μm)	D50(μm)	D90(μm)
Cement (C)	Grey	1.87	21.67	67.69
SMF1	Greyish brown	0.49	1.35	9.60
SMF2	Reddish brown	0.13	0.64	2.01
SMF3	Dark brown	0.66	2.59	22.68

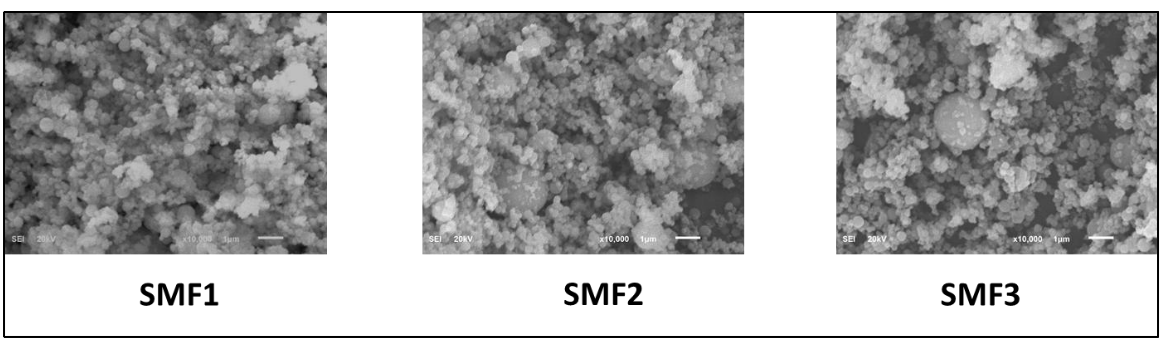

Figure 8 SEM of raw materials

3.2 Specimen preparation and curing

This thesis comprises two main parts. In the first part, SMF2 was used to prepare four distinct paste samples with varying OPC-to-SMF ratios of 100:0, 90:10, 80:20, and 70:30. A w/b ratio of 0.3, determined through trial mixes, was used for all samples. The required quantities of OPC, SMF, and mixing water were precisely measured. Initially, the OPC and SMF were dry mixed, followed by the addition of water, and then wet mixed for approximately 2.5 minutes until uniformity was achieved.

The prepared paste was cast into lubricated cubic steel molds of 50 mm dimensions in two layers, with each layer subjected to vibration for 5 seconds. The samples were covered immediately after casting and de-molded after 24 hours to prevent moisture loss. Instead of traditional water curing, avoiding the risk of leaching during the curing phase, the samples were wrapped in burlap, as shown in Figure 10, to maintain a moist environment. Curing was conducted for 28 days by regularly sprinkling water on the burlap at a controlled temperature of 23 ± 2 °C, ensuring optimal conditions without compromising sample integrity. Table 2 provides the mix design of these paste samples.

In the second part, three grades of SMFs, distinguished by their chemical compositions, were utilized to prepare four paste samples with OPC-to-SMF ratios of 100:0 and 80:20, maintaining the same W/B ratio of 0.3. The mixing process was conducted in a HOBART UTEST mortar mixer, as shown in Figure 9. The required OPC, SMF, and water quantities were carefully measured. Initially, OPC and SMF were dry mixed for 2 minutes at 62.5 rpm. The mixer was then stopped to scrape and mix the bottom layers using a trowel, followed by an additional minute of dry mixing at the same speed.

Figure 9 HOBART UTEST mortar mixer

Next, 70–80% of the water was added, and the mix was blended for 2 minutes at 62.5 rpm. The remaining water was then incorporated and mixing continued for 1 minute at the same speed. Subsequently, the speed was increased to 125 rpm for 1 minute. Hand mixing was performed with a trowel to ensure uniformity, and a final minute of mixing at 125 rpm completed the process.

The paste was cast into lubricated cubic steel molds of 25 mm × 25 mm × 25 mm size and subjected to 5 seconds of vibration. The samples were covered to prevent moisture loss, de-molded after 24 hours, and cured using traditional water curing at a controlled temperature of 23 ± 2 °C and steam curing at 90 ºC for 24 hours, as shown in Figure 10. The mix designs for these paste samples are also presented in Table 3.

Table 3 Mix design

Sample Code	Cement (wt%)	SMF (wt %)	W/B
Control(C)	100	0	0.3
SMF10	90	10	0.3
SMF20	80	20	0.3
SMF30	70	30	0.3
SMF1	80	20	0.3
SMF2	80	20	0.3
SMF3	80	20	0.3

(a) (b) (c)

Figure 10 Curing of samples a) burlap, b) traditional water curing, c) steam

3.3 Testing methods

3.3.1 Compressive Strength

Digital compression testing machine MATEST C55, as shown in Figure 11 with a loading rate of 1 KN/s, was used to test the compressive strength of the specimens following ASTM C109 [71]. The specimens were placed in the lower platens' center to avoid eccentric loading. In the first phase of this study, the strength was determined at 28 days of burlap curing and after three months of the leaching test, i.e., 118 days from casting. The respective control specimens (without leaching, WL) were also tested at the same age for comparison. Each specimen was tested in triplicate, and the average strength values were recorded.In the second phase, the testing was done 2 days (immediately after cooling of 24 hours steam curing) 7, 28, and 90-days steam cured followed by water curing.

Figure 11a) Compressive testing machine MATEST C55

3.3.2 Leaching Test

After burlap curing for 28 days, the specimens were put in leachate (deionized water) in a polypropylene vessel, ensuring that all the specimen surfaces were exposed to leachate, as shown in Figure 12. A mesh was used to subject the bottom side of the specimen to leachate, as shown in Figure 12. A ratio of 10 cm was maintained between the leachate volume and the external geometric surface. The test was performed at 25 °C over a 90-day period, with leachate samples collected at intervals of 2 hours and at 1, 2, 3, 4, 5, 19, 47, and 90 days. The leachate was replaced after each sampling. 50 mL of leachate sample was collected for ICP analysis. Then, 2 mL of 70% HNO_3 per 50 mL of leachate was added to the leachate to ensure that the metals were in the soluble form, preventing interference during ICP analysis. Finally, the samples were tested for Mn and Ca content using an ICAP6300 Duo thermo scientific ICP spectrometer. The tests were performed as per ANSI/ANS-16.1-2003 standard.

In parallel, three replicas of each specimen type were wrapped with polyethylene sheets to cure under normal conditions. Consequently, letters L and WL were added at the end of the specimen designation (nomenclature) to represent specimens after leaching and without leaching, respectively. For example, SMF10-L90 represents a specimen with 10% SMF subjected to leaching for 90 days, followed by 28 days of burlap curing. This nomenclature ensures clarity and consistency in identifying and discussing the various specimens and their respective treatments throughout the study.

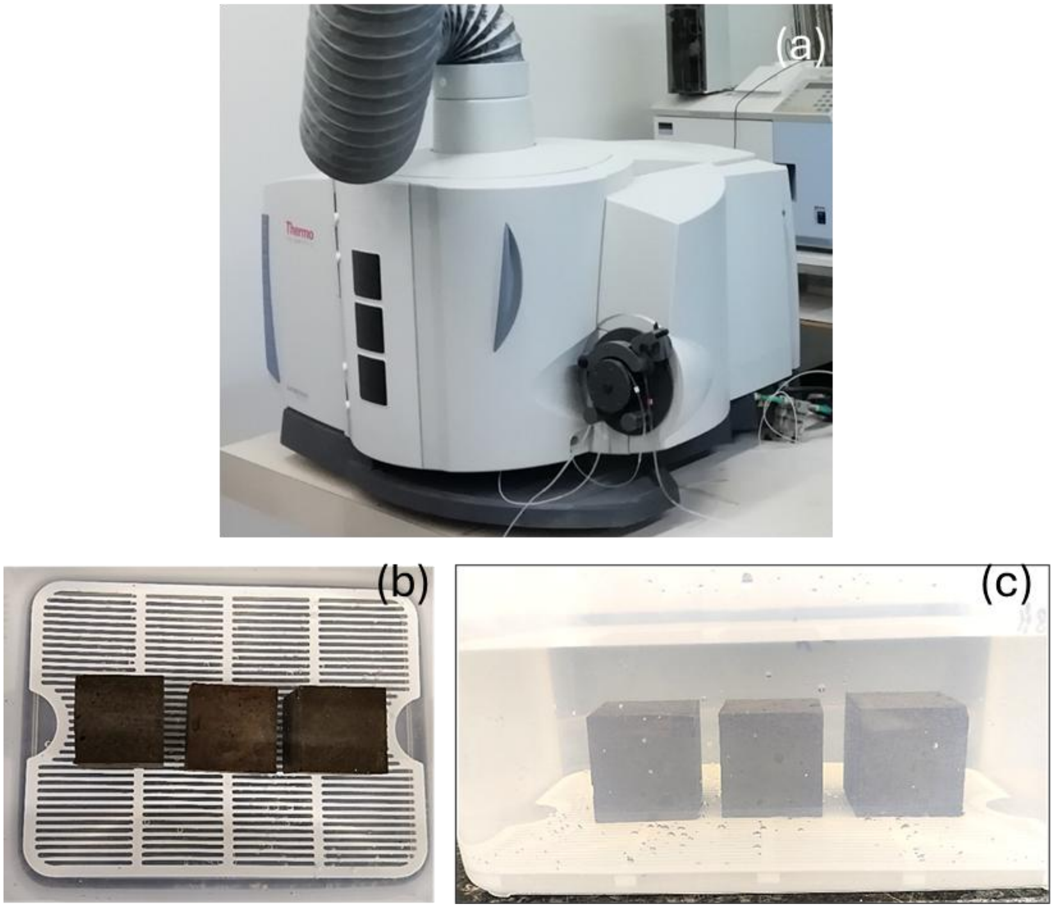

Figure 12 a) ICP OES instrument ICAP6300 DUO, Specimens in deionized water. b) Top view and c) side view

3.3.3 Morphological and Mineralogical Investigation

3.3.3.1 SEM/EDX (Scanning Electron Microscope/ Energy dispersive X-ray Spectroscopy) Analysis

SEM was employed using JEOL JSM-6610LV (Figure 13) to study the microstructural properties, including morphology, elemental composition, and bonding within the matrix contributing to the material's mechanical properties. The fractured samples were selected from the specimens tested for mechanical properties, and then the samples were prepared for SEM analysis. The solvent replacement method was used to dry the fractured specimens to preserve the 28-day hydration age. The samples were immersed in the isopropanol solution for 24 h, followed by vacuum-drying in a desiccator [72][73]. This drying ensures high-quality imaging as the moisture can affect the electron imaging. Furthermore, the specimens were coated with a thin conductive gold layer using a sputter coater, as shown in Figure 13. This layer reduces the charging effects from the electron beam and enhances image clarity.

EDS/EDX was conducted alongside SEM analysis to study elements' elemental composition and distribution within the samples selected area. For EDS, we do not need to prepare specimens separately; the analysis is directly done on SEM specimens. It provides a detailed elemental map, which is crucial for understanding SMF's influence on the matrix's hydration products. EDS analysis involves both elemental mapping and spot analysis. The former provides spatial visualization of elements like Ca, O, Mn, SI, and so on and reveals the dispersion patterns of the elements and their integration within the sample. The latter gives the precise quantification of the elemental composition at a specific point of interest.

(a) (b)

Figure 13 a) Gold Coating specimens to be investigated for SEM/EDX, b) SEM/EDX instrument JEOL JSM-6610LV

3.3.3.2 XRD (X-ray Diffraction) analysis

XRD analysis is a nondestructive analytical technique used to identify and quantify the crystalline phases present in materials. It measures the intensity and angles of diffraction of X-rays passing through the samples. This analysis is essential in providing valuable insights into the microstructural properties, such as the type and quantities of the hydration products formed. In this study, it was important to perform XRD to ascertain the influence of SMF on the mineral composition of paste samples.

After stopping the hydration, as discussed in SEM analysis, the fractured samples were carefully crushed and powdered using a mortar pestle. Then, the 100 μm passing sample powder was collected. Preparing the sample as a homogeneous, fine powder is crucial in XRD to produce accurate and reliable diffraction patterns, as larger or non-homogeneous particles could result in diffraction irregularities. The XRD analysis was done on these pulverized samples using an Ultima IV device manufactured by RIGAKU, as shown in Figure 14. The XRD data was collected in 2θ mode in the scan range of 5° to 65° at a scan speed of 2.5°/min.

Figure 14 RIGAKU Ultima IV XRD machine

3.3.3.3 TG/DTG (Thermogravimetric/ Differential Thermogravimetry) analysis

The thermogravimetric (TG/DTG) analysis is an analytical technique performed on PerkinElmer STA-6000, used to determine the weight losses as it is heated and phase transformations with temperature and to quantify the Portlandite (CH) and non-evaporable water (Wc) content. This provides insights into the thermal stability of the materials. The 10 °C/min heating rate under N_2 atmosphere and a temperature range of 30 °C to 1000 °C was observed. DTG is a derivative of TGA data, and it represents the rate of mass loss as a function of temperature, which helps to pinpoint the specific decomposition stages. The CH content was estimated from the decarbonation and dehydroxylation losses as calculated by Bhatty[74]. The Wc was determined by dehydration, decarbonation, and dehydroxylation losses. These losses were precisely determined by using the derivative curves and the corresponding weights[74][75–77]. The applicable equations for calculating CH and Wc are given as Eqs 2 and 3.

$$CH = 4.11LL_{dx} + 1.68\, L_{dc} \quad (2)$$

$$Wc = (L_{dh} + L_{dx}) + 0.41\, L_{dc} \quad (3)$$

where,

L_{dh} = dehydration weight loss (up to 250 °C)

L_{dx} = dehydroxylation weight loss (between 400 °C to 490 °C)

L_{dc} = decarbonation weight loss (between 600 °C to 720 °C)

Figure 15 TGA instrument PerkinElmer STA-6000

3.3.4 Reactivity test

The reactivity was studied through isothermal calorimetry testing, using the heat of hydration. It is a valuable method to study the hydration kinetics of cementitious materials, particularly when SCMs or chemical admixtures are added, as it gives us the chemical reactivity of the materials. However, a point to be noted is that it doesn't differentiate between pozzolanic and hydraulic reactivity. By tracking heat flow over time, isothermal calorimetry provides insights into how these materials affect the setting time, rate of reaction, and early-age strength development in concrete. Understanding these parameters is crucial, as they help design mixes that meet specific performance criteria while minimizing environmental impact.

This test was performed using the Calmetrix ICal 8000H, as shown in Figure 16. This test is performed in the following steps:

- **Thermostat Temperature Setting**: The test begins by setting the thermostat temperature of the calorimetry instrument to a target value of 40 °C and 23 °C, in accordance with standards ASTM C1897-20, ASTM C1702, and RILEM TC 267-TRM (Phases 1, 2, and 3)[78–80] .After setting the desired temperature, the instrument is left to stabilize for a minimum of 24 hours to ensure accurate and consistent conditions throughout the test.
- **Material Preparation and Weighing:** The materials are prepared and weighed precisely. This study used a total mass of 50 grams, consisting of an 80:20 ratio of OPC to SMF, w/b ratio of 0.3 was fixed. The mixing water must have the same temperature as the calorimetry instrument to prevent any temperature fluctuations during mixing.
- **Preconditioning of Water:** To match the calorimeter's temperature, the measured quantity of water is placed in sealed containers within the instrument for 2 to 3 hours. This step, known as "preconditioning of water," ensures that the water reaches a stable temperature before mixing, contributing to the consistency of the hydration reactions observed during testing.
- **Mixing the Materials:** After preconditioning, the materials are hand-mixed with the preconditioned water using a spoon, ensuring thorough mixing. Care is taken to scrape all material from the bottom and sides of the container to ensure uniformity. Once

mixing is complete, the spoon is left in the sealed container, as shown in the setup instructions, preventing any disturbance to the sample.

- **Sample Insertion and Data Logging:** The prepared sample is finally placed into the I-Cal calorimeter. The specific mix design parameters are entered into the instrument, and data logging is initiated. This enables continuous monitoring of heat flow, allowing for assessing the hydration activity and reactivity of the SCM in the mixture over time.

This standardized procedure ensures reliable and reproducible results when assessing the reactivity of supplementary cementitious materials in cementitious systems.

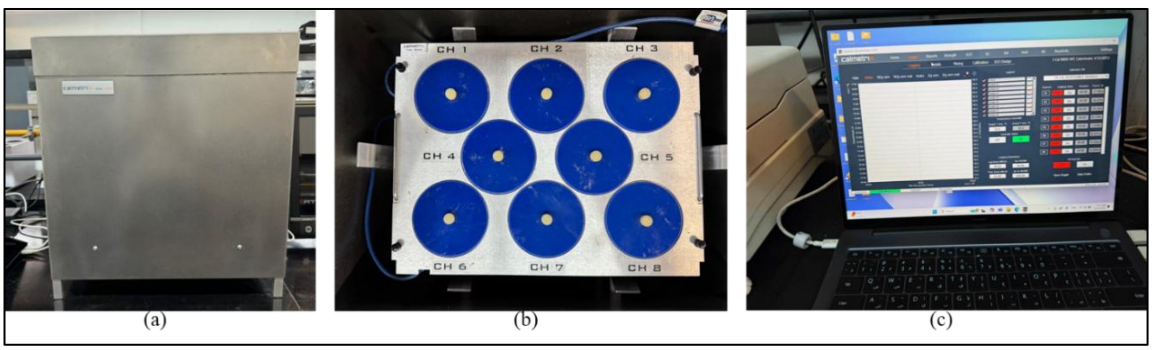

Figure 16 a) Calorimetry Instrument Calmetrix ICal 8000H b) inside view c) data logger

3.3.5 Flow table test

The flow table test is a method used to determine the workability or consistency of a cement paste or mortar. ASTM C230/C230M and ASTM C1437 are the standards applicable to perform this test [81,82]. The former outlines the specifications for the flow table apparatus, while the latter provides the detailed procedure for testing the flow of hydraulic cement mortar.

Preparation of Equipment and Materials: The primary equipment required for the test includes a flow table, a flow mold, a tamping rod, and a scale for measuring the flow diameter. As specified in ASTM C230, the flow table is a flat, circular surface with a diameter of 760 mm (30 in) and a rim height of 50 mm (2 in). It should be mounted on a stable, non-vibrating base and capable of being raised and dropped repeatedly. The flow mold is a truncated cone with a height of 100 mm (4 in), a top diameter of 100 mm (4 in), and a bottom diameter of 70 mm (2.75 in). A standard tamping rod, 16 mm (5/8 in) in diameter and 610 mm (24 in) long is used to compact the mortar into the mold. Before starting the test, the mortar or cement paste is prepared by mixing a specified ratio of cement, water, and possibly sand, depending on the specific test requirements. The mix should be homogeneous and free of air pockets. The water-to-cement ratio and the mix proportions should be based on the desired consistency or workability of the mortar, which is often indicated by the flow value expected in the test.

Filling the Mold: Once the mortar is prepared, the flow mold is placed in the center of the flow table. The mold is then filled with the mortar in two layers. Each layer should be compacted using the tamping rod, with 25 taps per layer, to remove any air bubbles and ensure a consistent, dense mix. It is slightly overfilled after the mold is filled to account for any possible settlement. The surface of the mold should be leveled to ensure uniformity.

Performing the Flow Test: After the mold is filled and compacted, it is carefully removed from the surface of the mortar, taking care not to disturb the shape of the sample. As the mold is lifted, the cement paste or mortar spreads radially across the flow table. The flow table is then dropped to a fixed height (usually around 12.5 mm or 0.5 inches) by raising and letting it fall. The table is typically dropped 25 times within 15 seconds, allowing the sample to spread under the repetitive impacts.

Measuring the Flow: Once the mortar has spread on the table, four perpendicular diameters of the spread sample are measured with a caliper or ruler. The diameter of the spread is recorded in millimeters (mm). The flow value is calculated as the average of these four measurements. This value reflects the workability of the cement paste or mortar: higher flow values signify a more fluid and workable mix, whereas lower flow values indicate a thicker, less workable mix. The following formula is used to calculate the flow in percentage:

$$Flow(\%) = \frac{d_{avg} - d}{d} \times 100 \qquad (4)$$

Where,

d_{avg} = average or mean value of the recorded four readings in millimeters.

d = original inside base diameter in millimeters.

Clean-Up and Final Steps: After the test, the flow table, mold, and tamping rod should be thoroughly cleaned to remove any remnants of the test material. The flow table test may be repeated with different mortar mixtures or water-cement ratios to assess the impact of various adjustments on the mix's workability. If the mortar does not flow as expected, adjustments can be made to the water content or mix proportions to achieve the desired consistency.

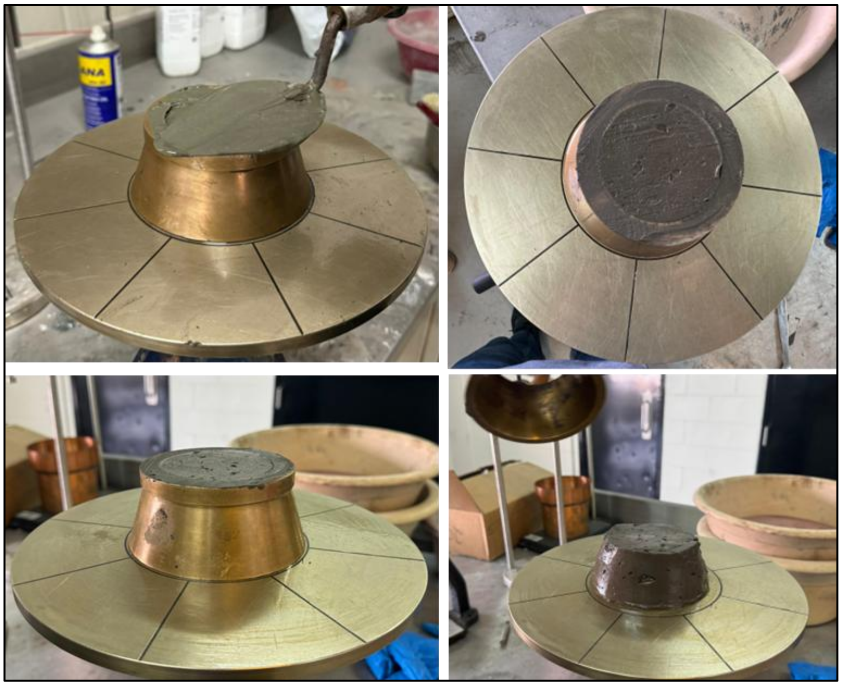

Figure 17 Flow table test

3.3.6 Setting Time

The setting time of hydraulic cement is a critical property that helps determine how long a cement mixture remains workable before it begins to harden. According to ASTM C191 – the standard test method for determining the time of setting of hydraulic cement by the Vicat needle – the setting time is measured in two key stages: the initial and final. These times indicate when the cement paste transitions from a plastic (workable) state to a solid (hardened) state, with the initial setting time marking the beginning of the hardening process and the final setting time marking when the cement is fully set and no longer plastic.

A Vicat apparatus is used to conduct the test. This apparatus consists of a vertical frame and a needle, typically 1 mm in diameter and weighing 300 grams. The needle is lowered onto the surface of the cement paste to measure the penetration at various stages. The test is performed with a cylindrical mold filled with freshly prepared cement paste. The paste is mixed with water at a specified water-to-cement ratio and placed into the mold. Once filled, the sample is allowed to rest briefly before the testing begins.

The test is carried out by placing the filled mold on a flat surface and using the Vicat needle to measure penetration at specific intervals. The initial setting time is determined when the needle penetrates the surface of the paste to a depth of 5-7 mm from the bottom. This marks when the paste has begun to stiffen but is still workable. The final setting time is identified when the needle fails to penetrate the paste by more than 0.5 mm, which indicates that the paste has fully hardened and is no longer in a plastic state.

The test is typically performed at a temperature of 20 ± 2°C (68 ± 3.6°F), which helps ensure consistency in results. The initial setting time is generally recorded as the time elapsed from when water is added to the cement until the needle penetrates the specified depth. Similarly, the final setting time is from mixing to when the needle fails to penetrate the sample. These measurements are usually expressed in minutes. For most cements, the initial setting time should be at least 45 minutes, and the final setting time should not exceed 600 minutes (10 hours). However, these times vary depending on the type of cement being used and the specific environmental conditions.

Once the test is completed, the results provide valuable information about the cement's handling characteristics. For example, the initial setting time refers to the duration, the cement remains workable and can be placed or finished. In contrast, the final setting time marks the point when the material has fully hardened and is capable of bearing load or undergoing further processing. Accurate measurement of setting times is essential for ensuring the cement is used within its optimal working window and achieves the required strength and durability for construction projects.

Figure 18 Vicat Apparatus

CHAPTER 4

Mechanical Behavior and Leaching Characteristics of Cementitious Composites Incorporating Silicomanganese Fume

4.1 Compressive Strength

Figure 19 shows the average 28-day strength of burlap-cured specimens. The trend shows that the 28-day strength with partial substitution of OPC by SMF up to 20% remains almost the same as the control. However, as the SMF content increased beyond 20%, a gradual decrease was observed, dropping from about 77 MPa at 20% to around 56 MPa at 30% replacement. This finding is consistent with the results reported by Gawah et al. [6]. The drop in the strength at higher SMF substitution levels could be due to the reduction in the primary hydration because of the reduced OPC content and limited/slower pozzolanic reactivity of SMF, resulting in an incomplete reaction at 28 days [49,83]. This is further discussed in the following paragraph in light of the long-term strength results. Moreover, the higher surface area of SMF can result in insufficient cement paste needed to make a strong matrix, which could also cause a loss of strength at higher substitution of OPC by SMF [6].

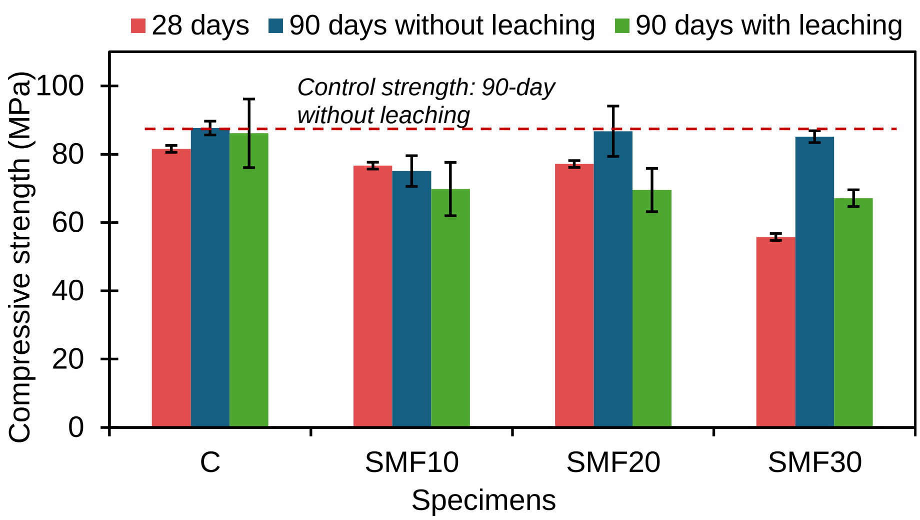

Figure 19 Compressive strength of control and SMF-substituted specimens

The strength of the specimens after 90 days of leaching (L), along with the compressive strength of respective control specimens (WL), is also compared in Figure 19. As expected, the strength of the WL specimens increased over time, potentially because of continuous hydration and the formation of secondary C-S-H by the pozzolanic reaction of SMF [83]. The strength of the control specimen C-WL increased slightly from 82 to 88 MPa (~7%), confirming additional hydration. However, a higher strength increase was observed in the SMF-substituted specimens, particularly in SMF20-WL and SMF30-WL. The strength of these specimens increased by about 13% and 52% compared to their respective 28-day strengths, respectively. This reflects the progression of additional pozzolanic reactions in SMF-substituted specimens over an extended period.

The strength of the specimens after leaching was found to be either comparable or less than the respective WL specimens. This could be linked to the potential leaching of unreacted Ca, CH, and Mn species, causing a reduction in the additional hydration and pozzolanic reaction [70,84–87], which in turn reduced the secondary hydrates formation (i.e., additional C-S-H gel) that would have otherwise contributed to a higher strength gain in concrete by the reaction of CH with amorphous silica in SMF. Thermogravimetric analyses can also substantiate the reduced CH content. The strength of the C-L and SMF10-L specimens was comparable to the C-WL and SMF10-WL, signifying that the higher content of OPC in these specimens resulted in sufficient hydration within 28 days. However, with the decreased OPC content and increased SMF content, the hydration degree at 28 days was reduced. Exposure to leachate after 28 days potentially reduced the degree of additional hydration and pozzolanic reaction, resulting in lesser strength gains. This effect was prominent in SMF30 where SMF30-L showed about only 20% increase in strength compared to 52% for SMF30-WL from their 28-day strength.

It can be concluded that the 20% OPC replacement by SMF appears to be the optimum to ensure high 28 days strength. However, the 30% replacement of OPC by SMF without leaching also exhibited the strength equivalent to the control specimen at 118 days, as shown in Figure 19. This indicates the need for further investigation into the effects of substituting OPC with SMF beyond the 30% threshold.

4.2 Leaching testing

The leaching is driven by a concentration gradient between the paste samples' ion-rich pore solution and the deionized water (leachate) surrounding it. The leaching assessment of SMF-substituted cement paste specimens demonstrated remarkable resistance to Mn release, with minimal leaching occurring in the first two days, as shown in Figure 20a. No Mn leaching was observed after the initial two days, continuing through the 90-day of testing period. This suggests that only the surface-bound Mn leached out, with no internal leaching of Mn occurring. These results were also confirmed by EDX analysis, discussed in Sec. 3.3.1, as the amount of Mn in the L and WL specimens was found to be in the same range. This minimal leaching phenomenon can be linked to the stable chemical matrix of the cement paste with SMF and the effective immobilization of manganese ions within the paste matrix.

However, there was a leaching of Ca ions, as shown in Figure 20b and as suggested by the EDX results in Sec. 4.3.1, which form the secondary hydration products by reacting with SCMs [84]. The highest leaching of Ca occurred in control specimen C, with about 234 ppm of Ca leached out, followed by the SMF20, SMF10, and SMF30 with values of about 223 ppm, 176 ppm, and 133 ppm, respectively. Initially, the calcium (Ca) leaching was very low across all specimens, with the control (C) specimen showing the highest leaching rates at all ages. However, the Ca leaching increased significantly over time in all the samples because of the dissolution and diffusion of CH from the paste matrix into the deionized water. The higher leaching rate is directly linked to the replacement of the leachate after each sampling. A concentration gradient was maintained by continually refreshing the leachate, encouraging the continuous release of calcium ions from the specimens. Without this replacement, the leachate would have gradually become saturated with calcium ions, reducing the concentration gradient. As a result, the driving force for leaching would diminish, leading to a lower leaching rate over time. The saturation of the leachate effectively limits the extent of calcium ion release [85].

Notably, specimens with a 30% replacement of OPC by SMF exhibited better resistance to Ca leaching, with about 43% less Ca leached out from SMF30-L than the control specimen C-L. This better resistance can be linked to the pore-filling effect of SMF at higher concentrations, fewer Ca ions available as 30% of OPC was replaced by SMF, and the utilization of Ca in the secondary hydration products formation. The leaching of Ca is further discussed in light of XRD results in Section 4.3.2. This leaching was also evidenced by the drop in the compressive strength of the specimens used for leaching tests compared to those not used for leaching tests, as discussed in the previous section (Sec. 4.1).

These results affirm the environmental safety of SMF as an SCM, particularly regarding Mn leaching and its potential to improve the sustainability quotient of construction materials. However, the only concern while incorporating SMF in concrete should be that it must not come directly in contact with water or moisture over a long time because of the following reasons: the possible leaching of Ca ions, its slow strength gain, and the third is less dense or porous microstructure even after 90 days after initial burlap curing for 28 days.

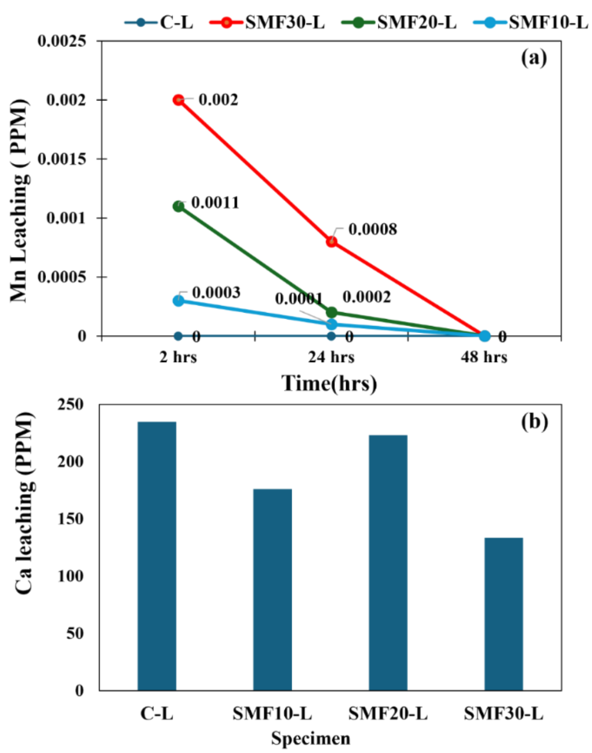

Figure 20 a) Mn leaching over time, b) Cumulative Ca leaching after 90 days of exposure

4.3 Microstructural and Phase transformation studies

4.3.1 SEM/EDX

Figure 21 illustrates the microstructural evolution of SMF-substituted cement paste samples at varying proportions after 28 days of burlap curing and after three months of leaching tests. At 28 days, a significant amount of SMF remains unreacted, as delineated by circles in Fig. 21a and 21d. This observation is more pronounced in samples with 30% SMF (Fig. 21a), attributable to the slow hydration kinetics. Consequently, this has led to a discernible reduction in compressive strength for SMF30, as discussed earlier [49,83,88].

The microstructural analysis of WL and L samples indicated progressive densification over time, with increased backscattered electron intensity, suggesting a more compact matrix than 28-day samples. The microstructure of WL specimens exhibited an increased density with minimal evidence of unhydrated particles in the SEM images, corroborating the gradual reactivity of SMF (Fig. 21b and 21e). This densification of the microstructure is evident by the gain in strength in these samples (SMF30-WL and SMF20-WL) due to the pozzolanic reaction of SMF. This confirms the reactive nature of SMF, which contributes to a more consolidated microstructure. Despite these advancements, some SMF particles remain unhydrated, potentially due to a low calcium-to-silica (C/S) ratio or inherently inert SMF constituents.

In contrast, specimens exposed to leaching solution displayed a porous microstructure, showing many unreacted particles as highlighted by circles (Fig. 21c and 21f). This is because of the slow reactivity of SMF and the possible leaching of Ca ions from the cement matrix. The EDX mapping was done to validate this argument, and representative results are shown in Figure 22. It is evident that the Ca content of the leaching specimens (SMF20-L) was much less than that of the WL specimens (SMF20-WL). This further validates the compressive strength and leaching results discussed in the previous sections.

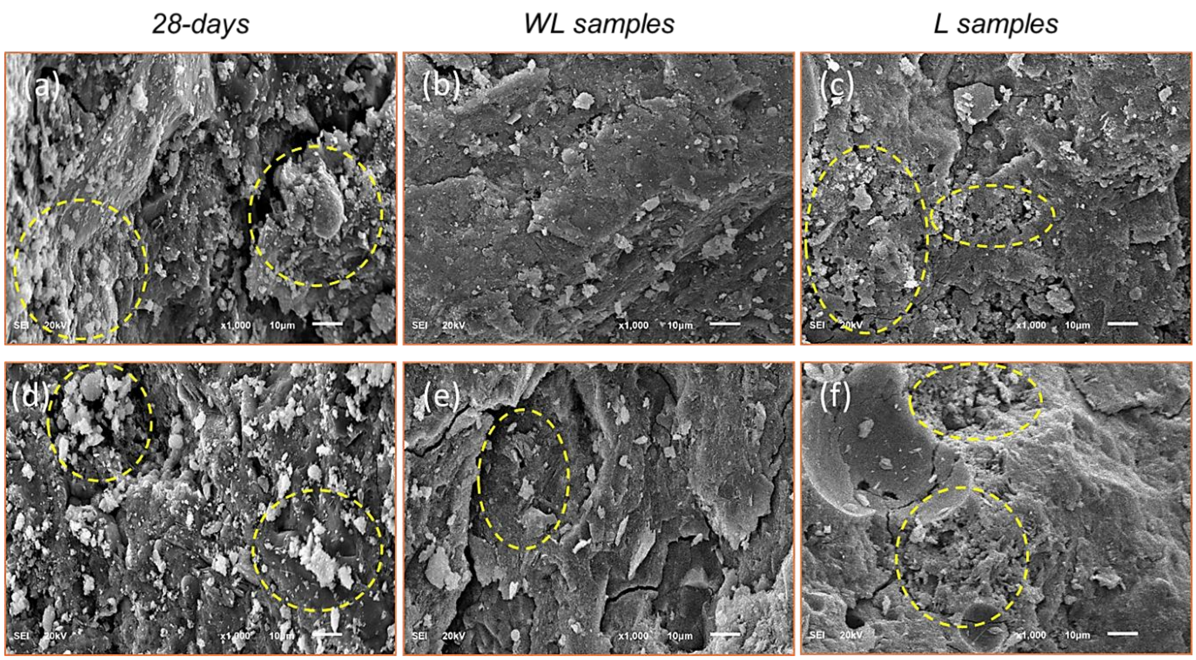

Figure 21. SEM images a) SMF30, b) SMF30-WL, c) SMF30-L, d) SMF20, e) SMF20-WL, and f) SMF20-L

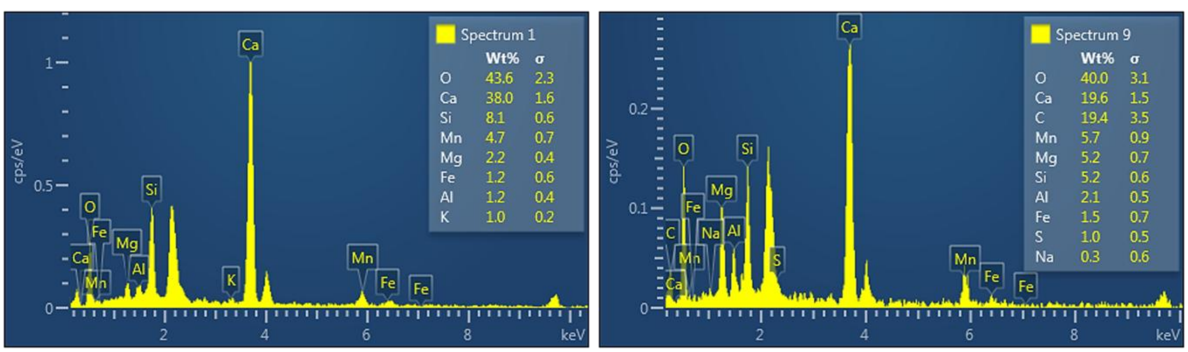

Figure 22.EDX mapping of without leaching SMF20-WL (left) and after leaching SMF20-L (right)

4.3.2 XRD

Figure 23 and Figure 24 show the x-ray diffractograms of the specimens at 28 days and 90 days after initial curing, respectively. The characteristic phases of hydrated OPC, such as CH, C-S-H gel, alite, and belite, were detected in the control sample. The 28-day X-ray diffractograms of SMF-substituted specimens showed no change in the peak position compared to the control specimen (C). Although the presence of SMF can impact the XRD pattern, these changes are subtle, especially for phases like quartz and calcite [89]. However, these specimens exhibited lower peak intensities, indicating a reduction in the crystalline phases. Notably, the CH peaks were more pronounced in the control specimen. As the percentage of SMF increased, the intensity of these peaks decreased. This reduction in intensity can be ascribed to the reduction in primary hydration due to the lower OPC content and the pozzolanic reaction of SMF. Subsequently, a diffuse hump was observed approximately between 15° to 25° in all the SMF-substituted specimens. This hump can be linked to the existence of amorphous phases, particularly silica, which lacks the long-range order typical of crystalline structures.

At 90 days after initial curing, the XRD patterns of the SMF samples, both with and without leaching, showed no distinct difference in peak positions, indicating that the same phases are present in both conditions. However, the intensity of the peaks varies, reflecting differences in the concentration and crystallinity of the phases. Furthermore, the hump initially present in 28-day XRD disappeared at this age, suggesting the amorphous phases present have undergone progressive reactions over time. This transformation is likely due to the pozzolanic reaction between the amorphous phases of SMF and the cement hydration products. The phases around 17° 2θ and 34° 2θ vary in intensity, suggesting a reduced portlandite content. This can be attributed to the pozzolanic reaction of SMF and the leaching of Ca in L samples, as discussed in section 4.2.

In SMF30-WL and SMF30-L samples, the identified peaks are consistent; however, the intensities of the portlandite content are slightly higher in SMF30-L at around 17° 2θ and

34° 2θ. This is because of the slower reactivity of SMF in leaching conditions as discussed in section 4.2. Furthermore, the quartz quantity is larger in SMF30-WL among all samples, possibly leading to strength gain at this age, as evidenced by the compression results. This phase appears responsible for the late gain in strength observed in the paste samples of SMF30-WL. The gradual increase in strength can also be attributed to the high amorphous nature of the material, particularly in the regions between 25° to 30° 2θ and 45° to 55° 2θ.

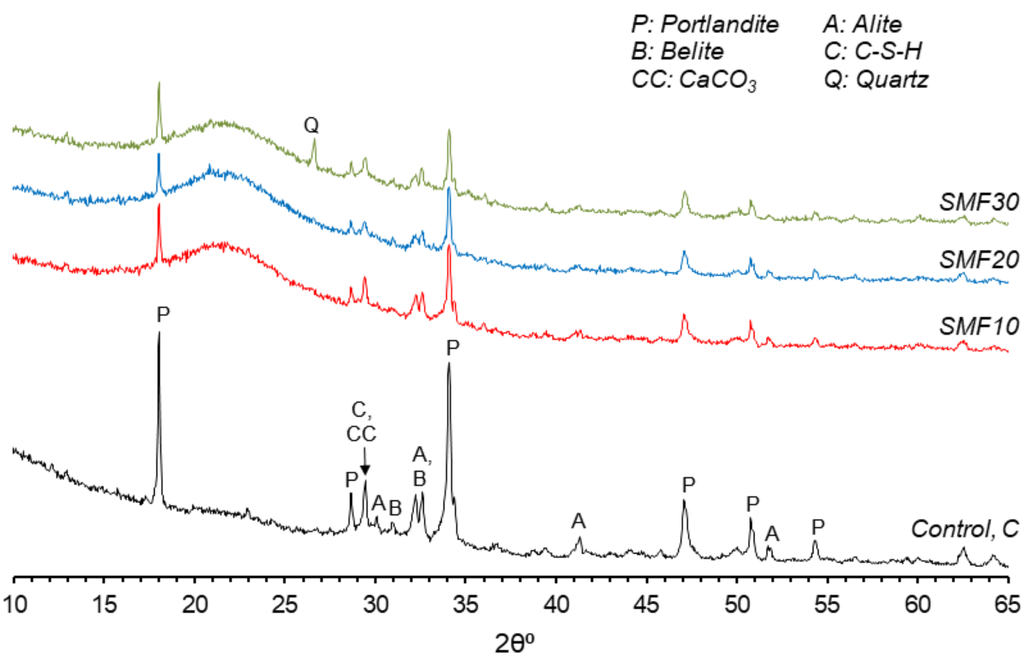

Figure 23.X-ray diffractograms of 28 days cured specimens

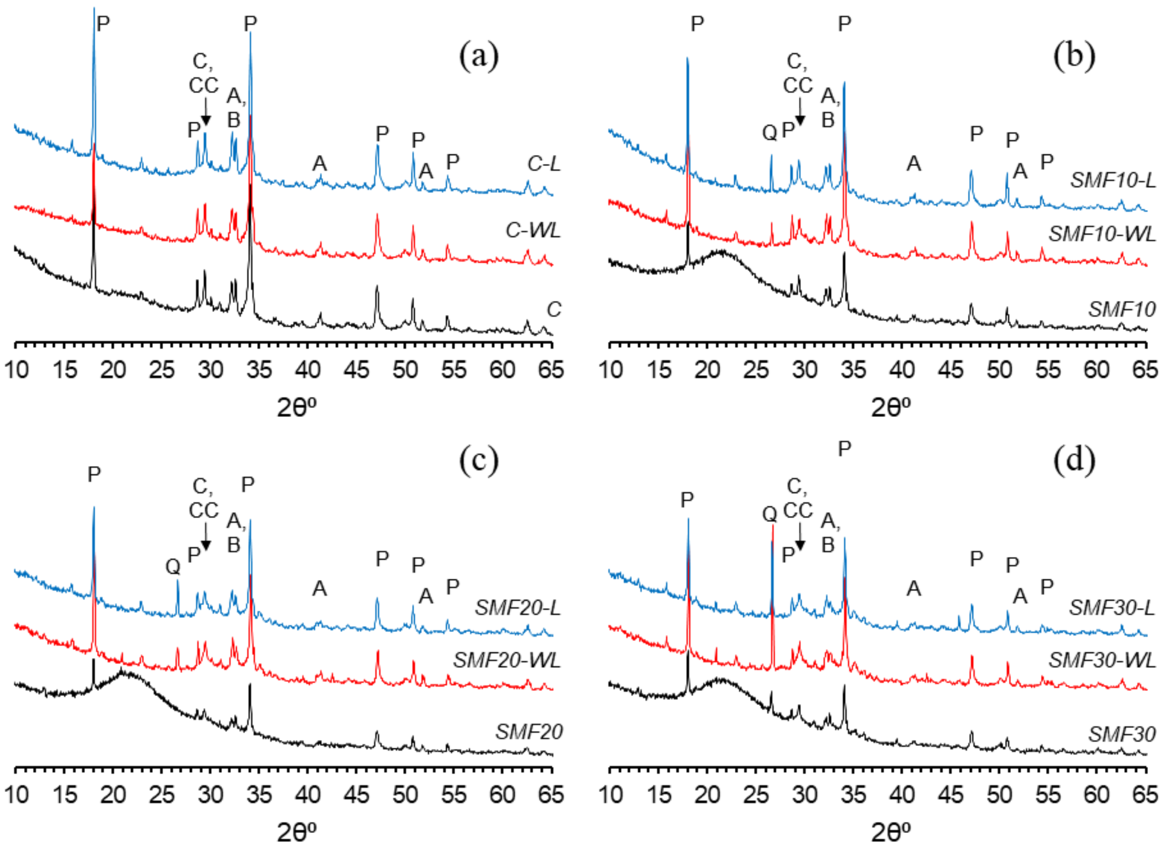

Figure 24 XRD comparisons of 28days, 90 days without leaching, and 90 days with leaching a) Control specimen, b) SMF10, c) SMF20, c) SMF30

4.3.3 TGA

The thermogravimetric analysis (TGA) conducted on the 28-day samples revealed distinct weight loss phases, as illustrated in Figure 25. The derivative thermogravimetry (DTG) curves exhibit three principal peaks. The initial peak occurred around 95 °C, which is attributed to gel water evaporation—a process known as dehydration. The second peak occurred around 440 °C due to portlandite decomposition. The final peak at around 670 °C corresponds to the decarbonation of calcium carbonate ($CaCO_3$). The specific temperatures associated with dehydration, dihydroxylation, and decarbonation were accurately determined from the DTG curves and used to calculate the content of Portlandite and non-evaporable water, as shown in Figure 26. In secondary hydration reactions, calcium hydroxide (CH) consumption leads to calcium silicate hydrate (CSH) gel formation. The reduced CH indicates the pozzolanic reactivity of SMF. Figure 26 shows a notable decrease in CH content from 20.25% in the control sample to 15.96% in the sample with 30% SMF substitution (SMF30), depicting the pozzolanic activity of SMF. Further, the increased amount of non-evaporable water in the specimens with SMF (Figure 26) shows a higher degree of hydration, leading to an enhanced and denser microstructure because more hydration products are formed.

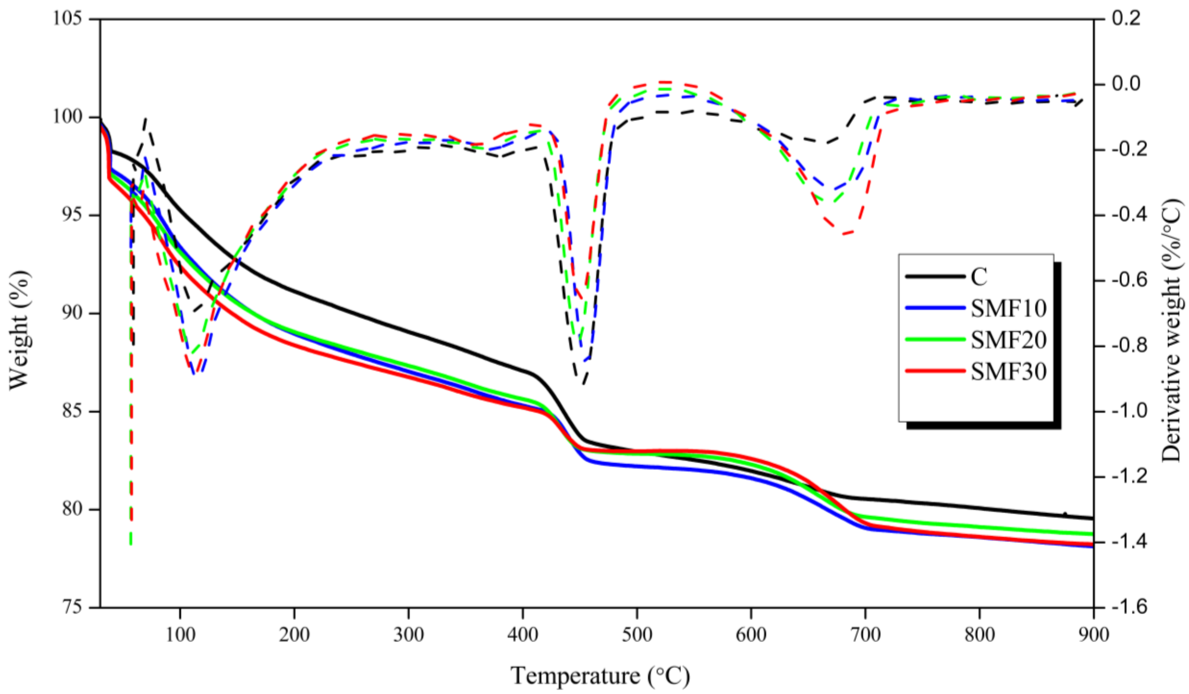

Figure 25. 28-day TGA weight loss curves

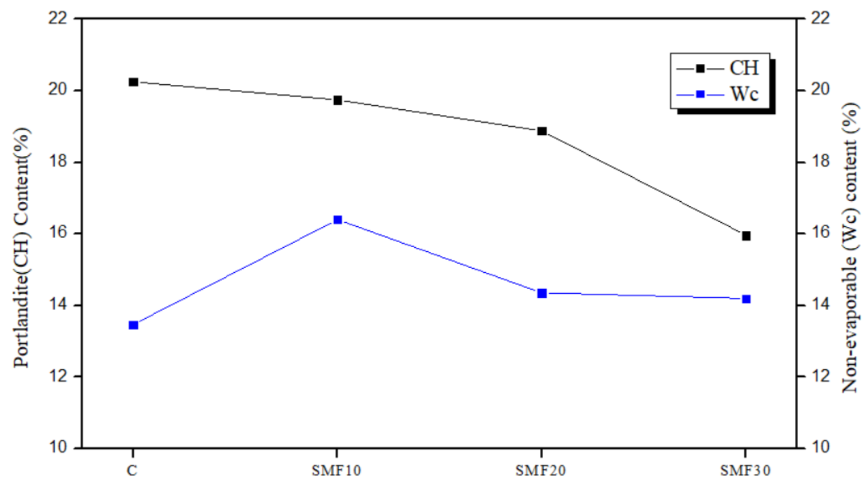

Figure 26.Amount of free Portlandite (CH) and non-evaporable water (Wc) content after 28 days of hydration

CHAPTER 5

Hydration Mechanism and Reactivity of cementitious Composites Incorporating different grades of Silicomanganese Fume

5.1 Setting Time and Flow Properties

Setting time is critical in understanding cement-based materials' workability and strength development, directly influencing the construction's transporting, placing, and finishing processes. Setting times are affected by the chemical composition of binders, W/B ratio, surrounding temperature, admixtures, or additives like SCMs.

The incorporation of SMF significantly increases cement paste's initial and final setting times, as shown in Table 4. The 20% replacement of cement by SMF1, SMF2, and SMF3 has shown a 1.875, 1.67, and 1.75 times increase in initial setting times and a 1.66, 1.5, and 1.64 times increase in final setting times, respectively, as compared to the control specimen. This trend indicates a consistent delay in the setting times with SMF inclusion. The SMF2 has the least amount of silica and hence has shown less retardation of setting times.

This increased setting times can be linked to several factors: the pozzolanic reactivity (reaction with portlandite) of SMF to form C-S-H gel; this reaction is relatively slower than the initial hydration of cement responsible for the early age setting and strength development. Secondly, the SMF dilutes the clinker, and the clinker phases are responsible for early strength gain in the mix, resulting in delayed initial formation of the binding matrix [90]. Furthermore, due to high surface areas of SMF and potential water absorption, the availability of free water in the mix is reduced, which could affect the mobility of ions and delay strength development.

Flowability is a critical property of cementitious composites, as it directly influences ease of placement, workability, and construction efficiency. This study evaluated the effect on flowability due to the incorporation of SMF, and the results are shown in Table 4. A w/b ratio of 0.3 was kept constant throughout the study to ensure consistency across all tests.

As illustrated in Table 4, the results indicate that the control(C) specimen exhibited the maximum flowability, demonstrating a flow diameter of 200 mm. However, among the SMF-containing mixtures, SMF1 displayed the lowest flowability, with a flow diameter of only 173 mm. In contrast, mixtures with SMF2 and SMF3 showed comparable flowability to the control specimen, with flow diameters of 191 mm and 196.6 mm, respectively. The flow decreased by including SMF because of the fineness and high surface area, increasing the water demand in the mix.

Table 4 Setting times and flow properties

Specimen	Setting time(minutes)		Flow	
	Initial	Final	mm	%
Control,C	120	280	200	100
SMF1	225	465	173	73
SMF2	200	420	191	91
SMF3	210	460	196.6	96.6

5.2 Compressive Strength

Figure 27 illustrates the compression testing of paste specimens (control and incorporating SMF) subjected to water curing for 7, 28, and 90 days. Across all specimens, strength increases with curing time, consistent with the prolonged hydration of cement and pozzolanic reactions. The control mix (C) achieves the highest compressive strength at all ages with values of approximately 70 MPa, 80 MPa, and 84 MPa respectively. In contrast, the performance of SMF-modified mixes varies depending on the specific SMF properties. SMF2(the finest of all grades) demonstrates the best performance among the modified mixes, with compressive strength comparable to the control at 90 days. On the other hand, SMF1 and SMF3 show lower compressive strength at both curing intervals, indicating that the variations in chemical composition, reactivity, and fineness of SMF significantly influence the strength development. This is consistent with the reactivity studies in the next section (section 5.3).

The control specimen's superior performance can be ascribed to its higher clinker content, which leads to rapid hydration and early-age strength development. However, the samples incorporating SMF have shown lower strengths at 7 and 28 days but comparable strength at 90 days by SMF2. This could be because of the pozzolanic reactivity SMF, slower than initial rapid hydration reactions, and the lower clinker percentage compared to C because the SMF replaces 20% of cement.

The steam curing process involves several distinct stages: the delay period, heating period, treatment period, and final cooling period. The delay period is the initial stage during which the specimens are undisturbed before heating begins. According to researchers, this period typically lasts between 0.5 to 5 hours. The heating period follows, during which the specimens are gradually heated to reach the desired target temperature. Once the target temperature is achieved, the treatment period begins at 90 ºC in our study, where the specimens are maintained at this constant curing temperature for the required duration. Finally, the cooling period reduces the specimens' temperature to normal atmospheric levels. Each of these stages plays a vital role in ensuring the effectiveness of the steam curing process, as they influence the material's internal structure and mechanical properties of the cured material [91].

Figure 28 compares the compression testing of paste specimens subjected to 2-day steam curing with those subjected to 28-day water curing. The results indicate that the control specimens achieved approximately 67% of the strength of the 28-day water-cured samples. In contrast, the steam-cured specimens incorporating SMF demonstrated significantly higher strength gains, achieving 89%, 99%, and 109% of the 28-day water-cured strength for SMF1, SMF2, and SMF3, respectively.

While the overall strength of steam-cured specimens is lower than that of the water-cured control, the substantial strength gain observed in SMF-containing samples can be attributed to the enhanced reactivity of SMF under elevated temperatures during steam curing. This highlights the potential of SMF as an effective supplementary material in accelerating early strength development.

Figure 29 illustrates the compressive strengths of specimens subjected to 24 hours of steam curing at 90°C, followed by subsequent curing in either moisture or water until the specified 7, 28, and 90-day curing periods. The results reveal that the control and SMF3 specimens experienced a reduction in strength at 28 days compared to their 7-day strengths. In contrast, the SMF1 specimens demonstrated a noticeable increased strength at 28 days, while SMF2 exhibited a slight improvement in strength over the same period.

The observed reduction in strength for the control and SMF3 specimens at later periods can be linked to the adverse effects of high-temperature steam curing. Research indicates that curing temperatures above 80°C can negatively impact the concrete microstructure, delaying ettringite formation and promoting the development of a porous structure, which contributes to reduced long-term strength[91]. Conversely, the strength improvement observed in SMF1 and SMF2 specimens suggests that their reactivity and continued hydration or pozzolanic activity during prolonged curing may counteract some of these adverse effects, enabling better strength at later ages.

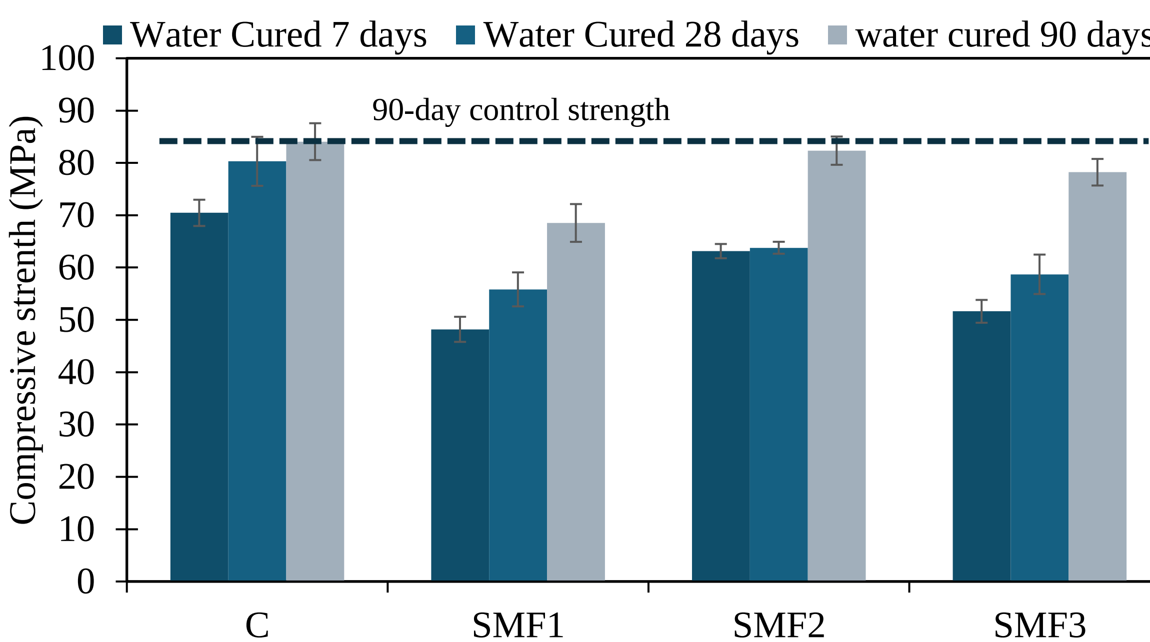

Figure 27 Compressive strength of control (C), SMF1, SMF2, and SMF3

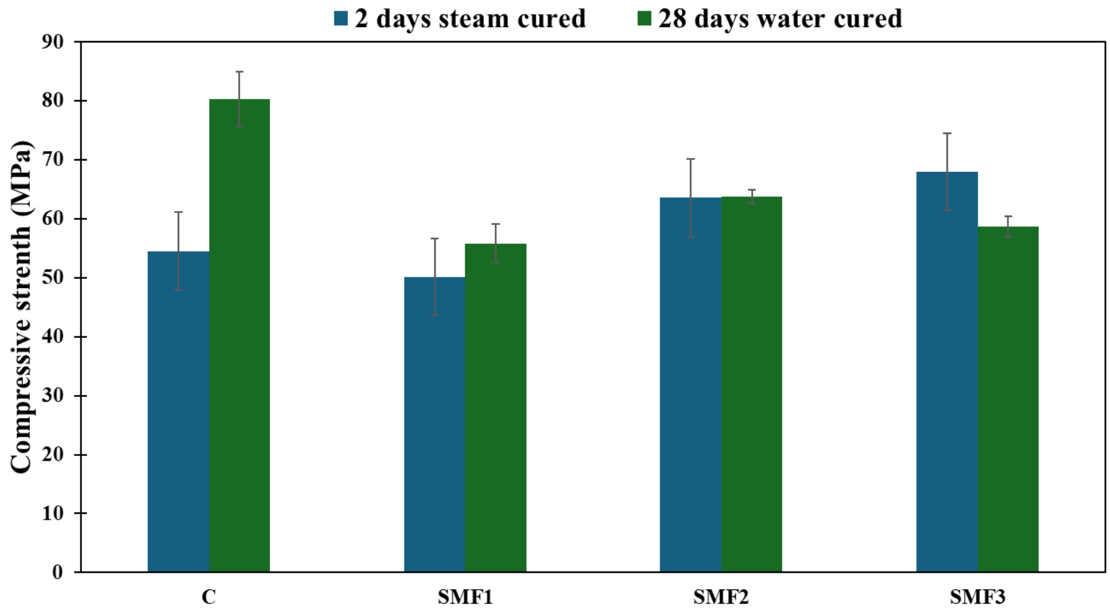

Figure 28 Comparison of steam-cured samples for 24 hours and water-cured at 28 days

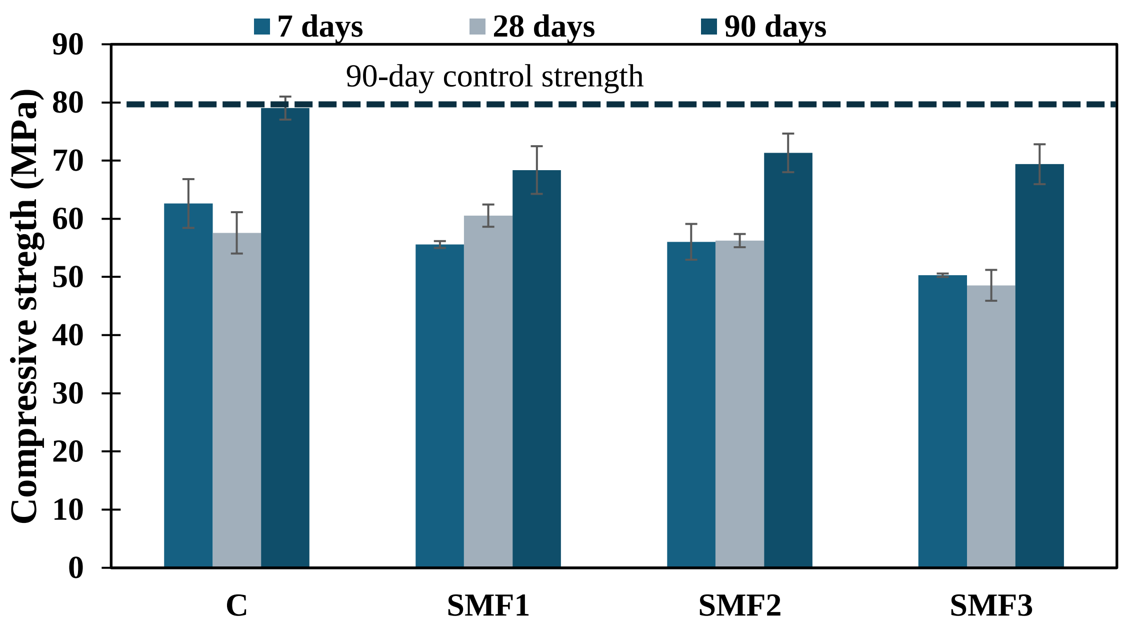

Figure 29 Steam curing for 24 hours followed by water curing for 7, 28, and 90 days

5.3 Reactivity using Isothermal Calorimetry

Isothermal calorimetry is a technique commonly employed to investigate the kinetics of cement hydration at constant temperatures. This method measures the heat flow released during hydration, enabling the determination of the rate of heat evolution. The total heat evolution can be quantified by integrating the heat flow over time. The heat evolution curve typically exhibits five stages of hydration: the initial reaction, the induction period, the acceleratory period, the deceleration period, and the period of slow continued reaction. Among these stages, the acceleratory period is critical as it corresponds to the rapid hydration of silicates, reaching the maximum heat evolution rate, which is crucial for setting. The deceleration period marks the transition from chemical control to diffusional control, as indicated by a reduction in heat flow [92].

Figures 30(a) and 30(b) present the calorimetry test results at 23°C for paste samples with a fixed W/B ratio of 0.3. The results compare the control sample with three grades of silicomanganese fume (SMF1, SMF2, and SMF3). The control and SMF2 specimens show similar heat flow profiles, with a peak heat evolution rate observed around 7 hours. This indicates that SMF2 exhibits significant reactivity in terms of heat evolution during hydration. In contrast, SMF1 and SMF3 demonstrate lower heat flow rates, suggesting reduced reactivity and minimal chemical interaction during hydration. At an elevated temperature of 40°C, the calorimetry results depicted in Figures 31(a) and 31(b) reveal distinct trends. The control specimen exhibits the highest heat flow rate, characterized by a steep acceleratory and deceleration period, indicating an accelerated hydration process at higher temperatures. However, the SMF samples behave differently: SMF1 and SMF3 display similar heat flow rates, which are lower than the control, suggesting that these SMFs delay the hydration rate and extend the setting time. This behavior highlights their potential use in managing the early-age properties of concrete under specific conditions.

Overall, SMF2 is the most reactive grade among the tested SMFs, demonstrating a notable contribution to the hydration process. In contrast, SMF1 and SMF3 show limited interaction. At higher temperatures, the inclusion of SMFs tends to delay hydration and setting, which could be advantageous for controlling the performance of concrete. This behavior aligns with the setting time and flow properties, as discussed in section 5.2, and with the compressive test results in section 5.3. These findings underscore the importance of interpreting calorimetry results accurately to optimize the use of SCMs in concrete applications.

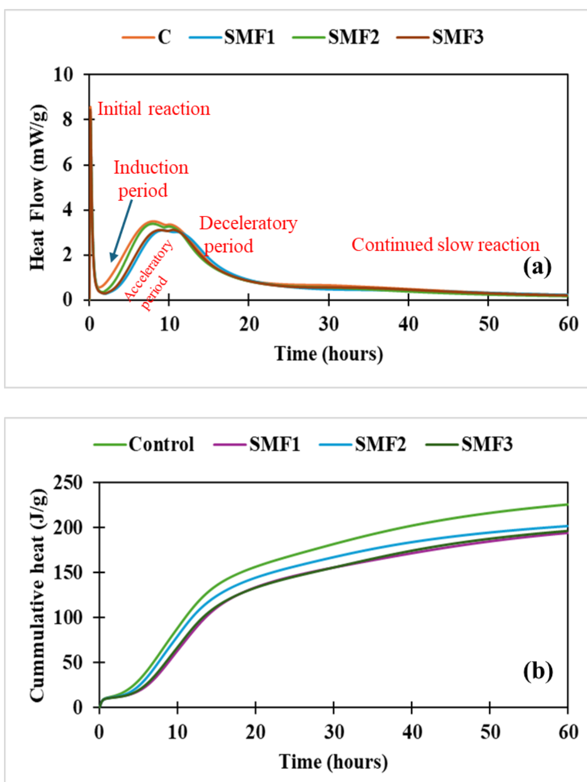

Figure 30 Isothermal calorimetry tests of cement pastes and SMF incorporated pastes at 23°C a) heat flow rate b) cumulative heat

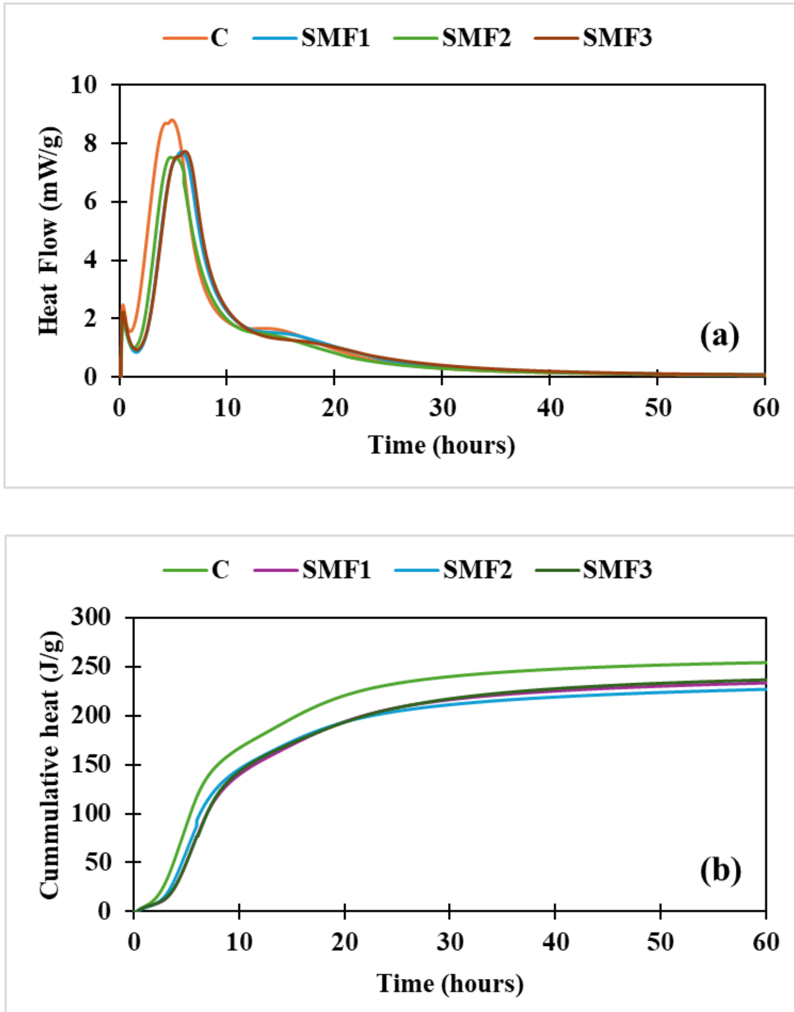

Figure 31 Isothermal calorimetry tests of cement pastes and SMF incorporated pastes at 40ºC

5.4 Microstructural Investigations

5.4.1 Scanning Electron Microscopy (SEM) Analysis

Figure 32 presents the SEM images of samples kept in water for 28 days. The microstructural analysis reveals that the control and SMF2 samples exhibit a dense microstructure with fewer visible pores, indicating well-developed hydration products and a compact matrix. In contrast, the SMF1 and SMF3 samples display a less dense microstructure with noticeable pores, suggesting incomplete hydration or reduced reactivity. This observation aligns well with the compressive strength results, where the control and SMF2 samples achieved higher strength values, reflecting their dense microstructure. Conversely, the reduced strength of SMF1 and SMF3 can be linked to the porous structure observed in their SEM images, which compromises the overall integrity and strength of the material.

Figure 33 shows the SEM images of specimens subjected to steam curing for 24 hours, followed by immersion in water for 28 days. The microstructure of these specimens appears uneven, with coarse pores compared to those cured exclusively in water. Steam curing accelerates the hydration process and promotes rapid hardening, leading to a more porous microstructure and irregular distribution of hydration products. This results in higher porosity, which contributes to enhanced strength at early ages however compromises long-term strength when compared to water-cured specimens, as discussed in compression testing(section 5.2) [93]. Furthermore, the utilization of SCMs mitigates the adverse effects of steam curing at later ages, as evidenced by the comparison of compressive strength [91,94,95].

The microstructural analysis highlights the significant impact of curing methods on the density and distribution of hydration products, which directly influence the strength of cement paste specimens. Water curing leads to a dense and uniform microstructure, as seen in the control and SMF2 specimens, promoting superior long-term strength. In contrast, steam curing accelerates hydration, improving early-age strength but resulting in a more porous and uneven microstructure that negatively affects long-term performance.

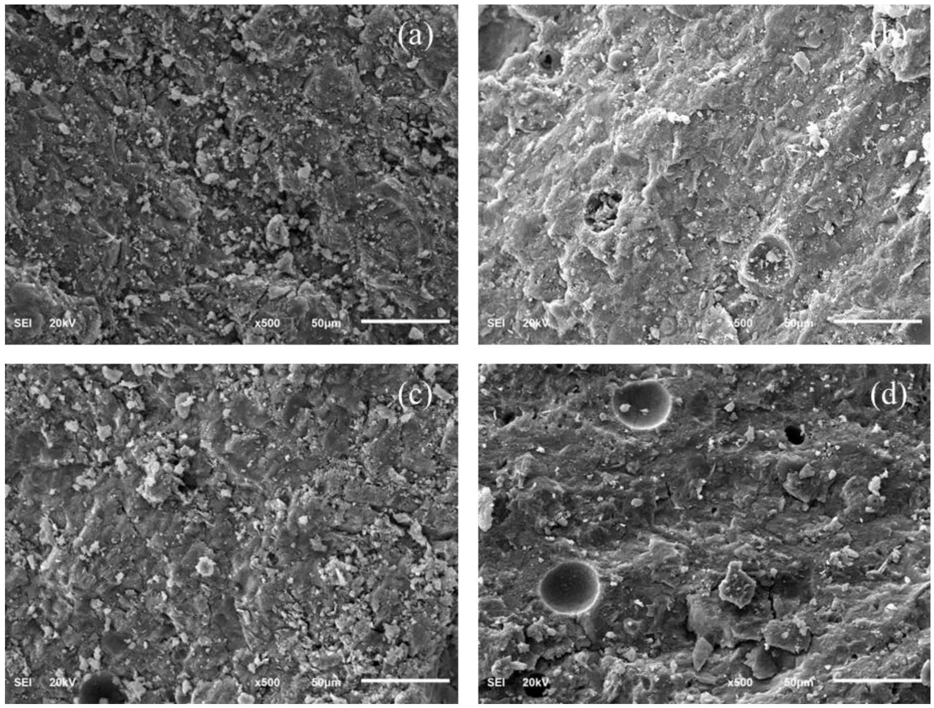

Figure 32 SEM of different specimens at 28 days water cured a) control (C), b) SMF1, c) SMF2, and d) SMF3

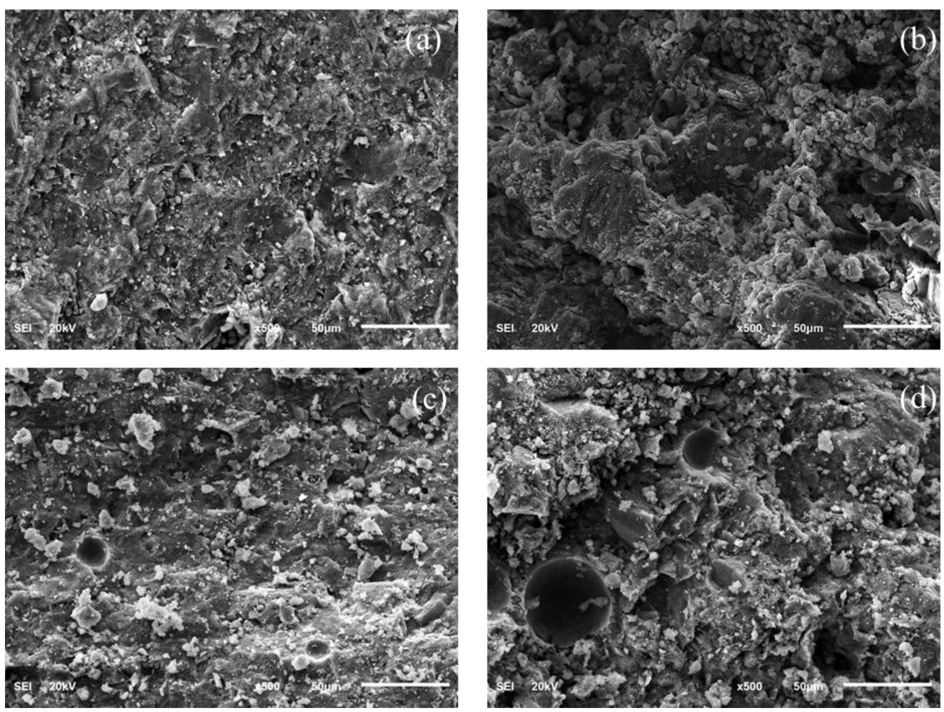

Figure 33 SEM of different specimens steam cured for 24 hours and then immersed in water until 28 days a) control (C), b) SMF1, c) SMF2, and d) SMF3

5.4.2 X-ray Diffractogram Analysis

Figures 34 and 35 present the X-ray diffractograms of specimens subjected to 28 days of water curing and 24 hours of steam curing (followed by immersion in water until 28 days), respectively. Under both curing conditions, the characteristic phases of hydrated OPC, namely CH, C-S-H gel, Alite, and Belite, were identified.

For the 28-day water-cured specimens, the XRD patterns of SMF-substituted samples showed no significant change in peak positions compared to the control specimen (C). However, quartz peaks were observed in SMF2 and SMF3, with a more pronounced presence in SMF3. While including SMF can subtly influence the XRD pattern, particularly for phases like quartz and calcite, these changes were minor. Additionally, the SMF-substituted specimens displayed lower peak intensities, indicating a reduction in crystalline phases, which suggests a more amorphous matrix.

Similarly, the XRD patterns of steam-cured specimens (steam curing for 24 hours followed by immersion in water until 28 days) showed comparable characteristic peaks. However, the peak intensities were notably lower than those of the 28-day water-cured specimens, indicating reduced portlandite content. This reduction in crystalline phases highlights the impact of steam curing, which accelerates early hydration but results in lower crystalline hydration products than prolonged water curing.

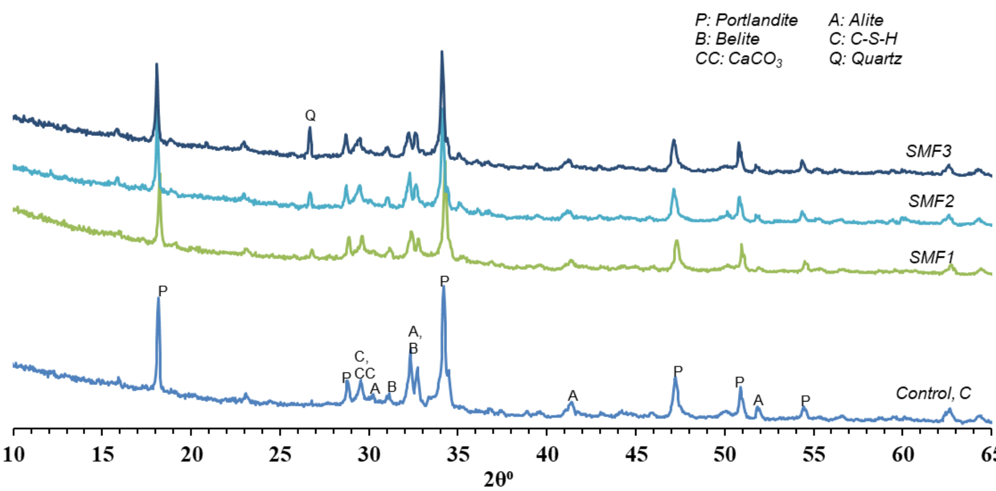

Figure 34 XRD of 28 days water-cured specimens

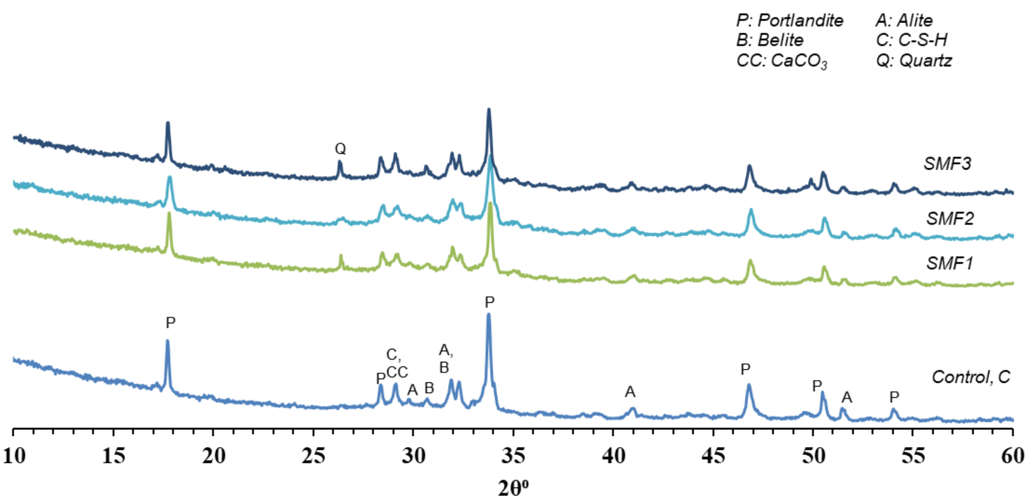

Figure 35 XRD of Steam cured for 24 hours and immersed in water until 28 days

5.5 Sustainability and Cost-Effectiveness of SMF as a Cement Replacement

Incorporating silicomanganese fume (SMF) as a supplementary cementitious material (SCM) in concrete production yields substantial economic and environmental advantages. Cement, a major constituent of concrete, significantly impacts production costs. By partially substituting cement with SMF, a cost-effective byproduct of the steel industry, material expenses decrease proportionally with the replacement percentage as shown in Table 6. This reduction enhances concrete affordability and promotes circular economy principles by utilizing an otherwise discarded material. Furthermore, the consistent cost of water across all mixes underscores the direct correlation between cement reduction and cost savings.

Furthermore, SMF replacement contributes to notable environmental benefits, particularly in mitigating the carbon footprint of concrete production. Cement manufacturing is a major contributor to global carbon dioxide emissions due to its energy-intensive processes. Conversely, SMF, as an industrial byproduct, has negligible associated emissions. Substituting cement with SMF significantly curtails overall carbon emissions per ton of concrete, with higher replacement levels yielding greater reductions as shown in Table 7. This aligns with sustainable construction practices and addresses climate change concerns and carbon neutrality goals.

Table 5 Unit cost and CO_2 emissions[6]

Material	Cement	Water	SMF
Units	Ton	Ton	Ton
Cost(SAR/unit)	600	5	0
CO_2 Emissions/unit (Kg)	900	1.9	8.1

Table 6 Reduction of CO_2 in percentage

Replacement Level	Cement CO_2 (Kg/ton)	SMF CO_2 (Kg/ton)	Water CO_2, (Kg/ton)	Total CO_2 (Kg/ton)	CO_2 Reduction (%)
C	900	0	1.9	901.9	0
SMF10	810	0.81	1.9	812.71	9.90
SMF20	720	1.62	1.9	723.52	19.80
SMF30	630	2.43	1.9	634.33	29.60

Table 7 Cost reduction in percentage

Replacement Level	Cement cost (SAR/ton)	SMF cost (SAR/ton)	Water cost, (SAR/ton)	Total cost (SAR/ton)	Cost Reduction (%)
C	600	0	4.5	604.5	0
SMF10	540	0	4.5	544.5	9.93
SMF20	480	0	4.5	484.5	19.85
SMF30	420	0	4.5	424.5	29.78

CHAPTER 6

Conclusions and Recommendations

6.1 Conclusions

A comprehensive study was conducted on the potential of SMF as SCM in a systematic way to evaluate its impact on the mechanical properties, microstructural evolution, and environmental suitability, mainly focusing on the leaching of Mn in the concrete by substituting 0%, 10%, 20%, and 30% of OPC with SMF and w/b ratio of 0.3 was used for preparing all the specimens. Furthermore, the reactivity of different grades of SMF was analyzed by replacing 20% of OPC with SMF1, SMF2, and SMF3, and their impact on the fresh properties, mechanical performance, and microstructural characteristics was evaluated. Based on the obtained results the following conclusions can be drawn.

- The positive impact of SMF on compressive strength was only for up to 20% replacement of OPC by SMF. Beyond 20%, it affected compressive strength negatively, as there was a noticeable decline in strength because of the slower reaction rate and unreacted SMF particles at higher percentages. This observation is critical in optimizing SMF content to maximize the beneficial effects on concrete strength without compromising the performance of concrete.
- Mn leaching assessment showed minimal release and below the standards, indicating effective immobilization of Mn within the cement matrix. This finding is crucial for incorporating SMF in concrete as it possesses negligible environmental risk concerning Mn contamination to groundwater or the surrounding ecosystem. Over time, higher percentages of SMF significantly reduce

Ca leaching, thereby improving the durability and strength of the cement paste specimens.

- Microstructural studies through SEM, XRD, and TGA revealed crucial insights into SMF-incorporated concrete's hydration products and structural evolution. SEM images depicted a denser microstructure with SMF contributing to the formation of additional hydration products. The gradual densification observed in samples over 90 days highlights the pozzolanic activity of SMF, although SEM images revealed some residual unreacted particles in higher substitution of OPC.
- The study highlights the potential of SMF to enhance the sustainability of concrete by reducing OPC consumption and mitigating CO_2 emissions associated with OPC production. Using industrial byproducts like SMF addresses environmental concerns and promotes resource efficiency and waste management in the construction industry. However, caution should be taken regarding prolonged exposure to moisture, as it may lead to calcium ion leaching and affect long-term durability.
- The inclusion of SMFs results in an increase in the setting times of cementitious mixtures. However, their effect on flow properties is minimal. This indicates that SMFs influence the hydration kinetics without significantly altering the workability of the mixtures.
- The effectiveness of SMF as a cement replacement is also influenced by the curing method employed. Specifically, specimens cured under burlap have demonstrated superior performance compared to those cured using water or steam.

- The reactivity of different grades of SMFs reveals that only SMF2 (finest of all grades with mean particle size 0.98 μm) demonstrates significant reactivity, with heat flow and cumulative heat values closely matching those of the control specimen, indicating active participation in the hydration process. In contrast, SMF1(mean particle size 3.37 μm) and SMF3 (mean particle size 8.18 μm) exhibit lower reactivity, reducing heat evolution. These results suggest that the finest grades of SMF are more effective in enhancing the hydration kinetics of cementitious mixtures, while coarser grades have a limited impact on the overall reactivity.

6.2 Recommendations

Future research avenues could explore advanced techniques for enhancing the reactivity of SMF, such as chemical activation or composite approaches with other SCMs. Long-term durability studies under diverse environmental conditions would provide further insights into the performance and sustainability of SMF-incorporated concrete over its lifecycle. Furthermore, detailed life cycle assessments (LCAs) could evaluate the environmental impacts and advantages of incorporating SMF in large-scale construction projects.

The feasibility of the synergistic use of SMF with other SCMs needs to be thoroughly assessed to explore their combined potential in enhancing concrete performance. Additionally, it is crucial to evaluate the industrial-scale applicability of SMF to determine its practicality and effectiveness in large-scale applications.

REFERENCES

[1] S.A. Miller, V.M. John, S.A. Pacca, A. Horvath, Carbon dioxide reduction potential in the global cement industry by 2050, Cem. Concr. Res. 114 (2018) 115–124. https://doi.org/https://doi.org/10.1016/j.cemconres.2017.08.026.

[2] P. Kathirvel, V. Saraswathy, S.P. Karthik, A.S.S. Sekar, Strength and durability properties of quaternary cement concrete made with fly ash, rice husk ash and limestone powder, Arab. J. Sci. Eng. 38 (2013) 589–598.

[3] S.-H. Jung, H.-S. Ryu, S. Karthick, S.-J. Kwon, Time and crack effect on chloride diffusion for concrete with fly ash, Int. J. Concr. Struct. Mater. 12 (2018) 14.

[4] S.-Y. Jang, S. Karthick, S.-J. Kwon, Investigation on Durability Performance in Early Aged High-Performance Concrete Containing GGBFS and FA, Adv. Mater. Sci. Eng. 2017 (2017) 3214696.

[5] N. Muhammad, A. Adeyemi, B.A. A., A.M. Arif, M.A. Hasan, I. Mohammed, Y.M. Olalekan, Strength, Microstructure, and Life Cycle Assessment of Silicomanganese Fume, Silica Fume, and Portland Cement Composites Designed Using Taguchi Method, J. Mater. Civ. Eng. 36 (2024) 4024190. https://doi.org/10.1061/JMCEE7.MTENG-17318.

[6] Q. Gawah, M.A. Al-Osta, M. Maslehuddin, M.A. Abdullah, M. Shameem, S.U. Al-Dulaijan, Development of sustainable self-compacting concrete utilising silico manganese fume, Eur. J. Environ. Civ. Eng. 27 (2023) 1897–1918. https://doi.org/10.1080/19648189.2022.2102083.

[7] J.G. Jang, S.M. Park, H.K. Lee, Physical barrier effect of geopolymeric waste form on diffusivity of cesium and strontium, J. Hazard. Mater. 318 (2016) 339–346. https://doi.org/10.1016/j.jhazmat.2016.07.003.

[8] B. Dawson, M. Spannagle, Intergovernmental Panel on Climate Change (Ipcc), 2020. https://doi.org/10.4324/9780203888469-41.

[9] S. Nie, J. Zhou, F. Yang, M. Lan, J. Li, Z. Zhang, Z. Chen, M. Xu, H. Li, J.G. Sanjayan, Analysis of theoretical carbon dioxide emissions from cement production: Methodology and application, J. Clean. Prod. 334 (2022) 130270. https://doi.org/https://doi.org/10.1016/j.jclepro.2021.130270.

[10] E. Benhelal, E. Shamsaei, M.I. Rashid, Challenges against CO2 abatement strategies in cement industry: A review, J. Environ. Sci. 104 (2021) 84–101. https://doi.org/https://doi.org/10.1016/j.jes.2020.11.020.

[11] NOAA Research, Carbon Cycle Greenhouse Gases, Glob. Monit. Lab. Earth Syst. Res. Lab. (2024) 3–5. https://doi.org/https://doi.org/10.15138/9N0H-ZH07.

[12] G. Feulner, Global Challenges: Climate Change, Glob. Challenges. 1 (2015) n/a-n/a. https://doi.org/10.1002/gch2.1003.

[13] R. Snellings, G. Mertens, J. Elsen, Supplementary Cementitious Materials, Rev. Mineral. Geochemistry. 74 (2012) 211–278. https://doi.org/10.2138/rmg.2012.74.6.

[14] D. Elzinga, S. Bennett, D. Best, K. Burnard, P. Cazzola, D. D'Ambrosio, J. Dulac, A. Fernandez Pales, C. Hood, M. LaFrance, Energy technology perspectives 2015: mobilising innovation to accelerate climate action, Paris Int. Energy Agency. (2015).

[15] A. Adesina, Recent advances in the concrete industry to reduce its carbon dioxide emissions, Environ. Challenges. 1 (2020) 100004. https://doi.org/10.1016/j.envc.2020.100004.

[16] P. Neeraja, S. Unnikrishnan, A. Varghese, A comprehensive review of partial replacement of cement in concrete, Mater. Today Proc. (2023). https://doi.org/10.1016/j.matpr.2023.05.070.

[17] H.J. Yang, M. Usman, A. Hanif, Suitability of liquid crystal display (LCD) glass waste as supplementary cementing material (SCM): Assessment based on strength, porosity, and durability, J. Build. Eng. 42 (2021) 102793. https://doi.org/https://doi.org/10.1016/j.jobe.2021.102793.

[18] S. Ahmad, H.R. Khalid, A.A. Shaqraa, A.A. Bahraq, M. Maslehuddin, S.U. Al-Dulaijan, Properties of natural pozzolan-based geopolymer concrete: effects of natural pozzolan content, type of alkaline activator, and silicate/alkali ratio, Eur. J. Environ. Civ. Eng. 27 (2023) 356–373. https://doi.org/10.1080/19648189.2022.2043941.

[19] E. Worrell, L. Price, N. Martin, C. Hendriks, L.O. Meida, Carbon dioxide emissions from the global cement industry, Annu. Rev. Energy Environ. 26 (2001) 303–329. https://doi.org/10.1146/annurev.energy.26.1.303.

[20] M. Nasir, M.A.M. Johari, M. Maslehuddin, M.O. Yusuf, M.A. Al-Harthi, Influence of heat curing period and temperature on the strength of silico-manganese fume-blast furnace slag-based alkali-activated mortar, Constr. Build. Mater. 251 (2020) 118961. https://doi.org/10.1016/j.conbuildmat.2020.118961.

[21] M.B. Ali, R. Saidur, M.S. Hossain, A review on emission analysis in cement industries, Renew. Sustain. Energy Rev. 15 (2011) 2252–2261. https://doi.org/https://doi.org/10.1016/j.rser.2011.02.014.

[22] N. MAHASENAN, S. SMITH, K. HUMPHREYS, The Cement Industry and Global Climate ChangeCurrent and Potential Future Cement Industry CO2 Emissions, in: J. Gale, Y.B.T.-G.G.C.T.-6th I.C. Kaya (Eds.), Greenh. Gas Control Technol. - 6th Int. Conf., Pergamon, Oxford, 2003: pp. 995–1000. https://doi.org/10.1016/b978-008044276-1/50157-4.

[23] Supriya, R. Chaudhury, U. Sharma, P.C. Thapliyal, L.P. Singh, Low-CO2 emission strategies to achieve net zero target in cement sector, J. Clean. Prod. 417

(2023) 137466. https://doi.org/https://doi.org/10.1016/j.jclepro.2023.137466.

[24] M. Schneider, The cement industry on the way to a low-carbon future, Cem. Concr. Res. 124 (2019) 105792. https://doi.org/https://doi.org/10.1016/j.cemconres.2019.105792.

[25] M. Hanifa, R. Agarwal, U. Sharma, P.C. Thapliyal, L.P. Singh, A review on CO2 capture and sequestration in the construction industry: Emerging approaches and commercialised technologies, J. CO2 Util. 67 (2023) 102292. https://doi.org/https://doi.org/10.1016/j.jcou.2022.102292.

[26] Hannah Ritchie and Max Roser, Global Carbon Budget (2023) – with major processing by Our World in Data. "Annual CO_2 emissions – GCB" [dataset]. Global Carbon Project, "Global Carbon Budget" [original data]., Https://Ourworldindata.Org/Co2-Emissions. (2023). https://ourworldindata.org/co2-emissions.

[27] C.S.I. IEA, Technology Roadmap Low-Carbon Transition in the Cement Industry, Fr. Geneva, Switzerland. IEA, Paris. (2018).

[28] B. Lothenbach, K. Scrivener, R.D. Hooton, Supplementary cementitious materials, Cem. Concr. Res. 41 (2011) 1244–1256. https://doi.org/https://doi.org/10.1016/j.cemconres.2010.12.001.

[29] B. Lothenbach, K. Scrivener, R.D. Hooton, Supplementary cementitious materials, Cem. Concr. Res. 41 (2011) 1244–1256. https://doi.org/10.1016/j.cemconres.2010.12.001.

[30] R. Snellings, P. Suraneni, J. Skibsted, Future and emerging supplementary cementitious materials, Cem. Concr. Res. 171 (2023) 107199. https://doi.org/https://doi.org/10.1016/j.cemconres.2023.107199.

[31] M.C.G. Juenger, R. Snellings, S.A. Bernal, Supplementary cementitious materials: New sources, characterization, and performance insights, Cem. Concr. Res. 122 (2019) 257–273. https://doi.org/10.1016/j.cemconres.2019.05.008.

[32] G.M. Kim, H.R. Khalid, H.J. Kim, H.K. Lee, Alkali activated slag pastes with surface-modified blast furnace slag, Cem. Concr. Compos. 76 (2017) 39–47. https://doi.org/https://doi.org/10.1016/j.cemconcomp.2016.11.009.

[33] J.L. Provis, Geopolymers and other alkali activated materials: why, how, and what?, Mater. Struct. 47 (2014) 11–25. https://doi.org/10.1617/s11527-013-0211-5.

[34] K.L. Scrivener, P. Juilland, P.J.M. Monteiro, Advances in understanding hydration of Portland cement, Cem. Concr. Res. 78 (2015) 38–56. https://doi.org/https://doi.org/10.1016/j.cemconres.2015.05.025.

[35] T. Matschei, B. Lothenbach, F.P. Glasser, The role of calcium carbonate in cement hydration, Cem. Concr. Res. 37 (2007) 551–558.

https://doi.org/https://doi.org/10.1016/j.cemconres.2006.10.013.

[36] K. De Weerdt, M. Ben Haha, G. Le Saout, K.O. Kjellsen, H. Justnes, B. Lothenbach, Hydration mechanisms of ternary Portland cements containing limestone powder and fly ash, Cem. Concr. Res. 41 (2011) 279–291. https://doi.org/https://doi.org/10.1016/j.cemconres.2010.11.014.

[37] M. Antoni, Investigation of cement substitution by blends of calcined clays and limestone, EPFL, 2013.

[38] A.C.P. Martins, J.M. Franco de Carvalho, L.C.B. Costa, H.D. Andrade, T.V. de Melo, J.C.L. Ribeiro, L.G. Pedroti, R.A.F. Peixoto, Steel slags in cement-based composites: An ultimate review on characterization, applications and performance, Constr. Build. Mater. 291 (2021) 123265. https://doi.org/https://doi.org/10.1016/j.conbuildmat.2021.123265.

[39] M.J. McCarthy, T. Robl, L.J. Csetenyi, Recovery, processing, and usage of wet-stored fly ash, in: Coal Combust. Prod., Elsevier, 2017: pp. 343–367.

[40] W.F. Cannon, Manganese—It Turns Iron Into Steel (and Does So Much More), USGS Miner. Resour. Progr. (2014) 3087. http://minerals.usgs.gov/minerals/pubs/.

[41] X. Sun, H. Hao, Z. Liu, F. Zhao, Insights into the global flow pattern of manganese, Resour. Policy. 65 (2020) 101578. https://doi.org/https://doi.org/10.1016/j.resourpol.2019.101578.

[42] T.G. Cota, L.M. de M.S. Cheloni, J.J.M. Guedes, É.L. Reis, Silico-manganese slag and its utilization into alkali-activated materials: A critical review, Constr. Build. Mater. 399 (2023) 132589. https://doi.org/https://doi.org/10.1016/j.conbuildmat.2023.132589.

[43] W. Razzaq, S. Elkatatny, H. Gamal, A. Samsuri, The utilization of steelmaking industrial waste of silicomanganese fume as filtration loss control in drilling fluid application, J. Energy Resour. Technol. 144 (2022) 23004.

[44] M.A. Khan, S.M. Wabaidur, M.R. Siddiqui, A.A. Alqadami, A.H. Khan, Silico-manganese fumes waste encapsulated cryogenic alginate beads for aqueous environment de-colorization, J. Clean. Prod. 244 (2020) 118867. https://doi.org/10.1016/j.jclepro.2019.118867.

[45] I. Kero, M.K. Naess, G. Tranell, Particle size distributions of particulate emissions from the ferroalloy industry evaluated by electrical low pressure impactor (ELPI), J. Occup. Environ. Hyg. 12 (2015) 37–44.

[46] I.N.A. Al-Duais, S. Ahmad, M.A. Al-Osta, M. Maslehuddin, T.A. Saleh, Properties of Alkali-Activated Concrete Made Using the Optimum Combinations of Precursor Materials and Activation Parameters, J. Mater. Civ. Eng. 36 (2024). https://doi.org/10.1061/jmcee7.mteng-16944.

[47] M. Nasir, M.A. Megat Johari, M. Maslehuddin, M. Olalekan Yusuf, Magnesium

sulfate resistance of alkali/slag activated silico-manganese fume-based composites, Constr. Build. Mater. 265 (2020) 120851. https://doi.org/10.1016/j.conbuildmat.2020.120851.

[48] S.K. Najamuddin, M.A. Megat Johari, M. Maslehuddin, M.O. Yusuf, Synthesis of low temperature cured alkaline activated silicomanganese fume mortar, Constr. Build. Mater. 200 (2019) 387–397. https://doi.org/10.1016/j.conbuildmat.2018.12.056.

[49] M. Nasir, M.A.M. Johari, M.O. Yusuf, M. Maslehuddin, M.A. Al-Harthi, Synthesis of alkali-activated binary blended silico-manganese fume and ground blast furnace slag mortar, J. Adv. Concr. Technol. 17 (2019) 728–735.

[50] Y.J. Arnoldussen, T. Kringlen Ervik, J. Samulin Erdem, I. Kero, M. Baarnes Eriksen, V. Skaug, S. Zienolddiny, Mechanisms of toxicity of industrially relevant silicomanganese dust on human 1321N1 astrocytoma cells: An in vitro study, Int. J. Mol. Sci. 20 (2019) 740.

[51] W. Razzaq, S. Elkatatny, A. Gowida, A. Samsuri, Application of Silicomanganese Fume as a Novel Bridging Material for Water-Based Drilling Fluids, ACS Omega. (2022). https://doi.org/10.1021/acsomega.2c05456.

[52] W. Razzaq, S. Elkatatny, H. Gamal, A. Samsuri, The Utilization of Steelmaking Industrial Waste of Silicomanganese Fume as Filtration Loss Control in Drilling Fluid Application, J. Energy Resour. Technol. 144 (2021). https://doi.org/10.1115/1.4051197.

[53] M. Nasir, M.A.M. Johari, M. Maslehuddin, M.O. Yusuf, M.A. Al-Harthi, Influence of heat curing period and temperature on the strength of silico-manganese fume-blast furnace slag-based alkali-activated mortar, Constr. Build. Mater. 251 (2020) 118961. https://doi.org/https://doi.org/10.1016/j.conbuildmat.2020.118961.

[54] M. Nasir, M.A. Megat Johari, M. Maslehuddin, M. Yusuf, Sulfuric acid resistance of alkali/slag activated silico-manganese fume-based mortars, Struct. Concr. 22 (2020). https://doi.org/10.1002/suco.201900543.

[55] S.K. Najamuddin, M.A. Megat Johari, M. Maslehuddin, M.O. Yusuf, Development of Sustainable Cementitious Binder Utilizing Silicomanganese Fumes, Springer Singapore, 2020. https://doi.org/10.1007/978-981-15-1616-0_29.

[56] M. Nasir, A. Adesina, A.A. Bahraq, M.A. Aziz, A.H. Mahmood, M. Ibrahim, M.O. Yusuf, Strength, Microstructure, and Life Cycle Assessment of Silicomanganese Fume, Silica Fume, and Portland Cement Composites Designed Using Taguchi Method, J. Mater. Civ. Eng. 36 (2024) 1–10. https://doi.org/10.1061/jmcee7.mteng-17318.

[57] G.R. Evans, L.N. Masullo, Manganese Toxicity, StatPearls Publishing, Treasure Island (FL), 2023. http://europepmc.org/abstract/MED/32809738.

[58] D. Hernández-Bonilla, A. Schilmann, S. Montes, Y. Rodríguez-Agudelo, S. Rodríguez-Dozal, R. Solís-Vivanco, C. Ríos, H. Riojas-Rodríguez, Environmental exposure to manganese and motor function of children in Mexico., Neurotoxicology. 32 (2011) 615–621. https://doi.org/10.1016/j.neuro.2011.07.010.

[59] Y. Kim, R.M. Bowler, N. Abdelouahab, M. Harris, V. Gocheva, H.A. Roels, Motor function in adults of an Ohio community with environmental manganese exposure., Neurotoxicology. 32 (2011) 606–614. https://doi.org/10.1016/j.neuro.2011.07.011.

[60] E. Pajarillo, I. Nyarko-Danquah, G. Adinew, A. Rizor, M. Aschner, E. Lee, Chapter Six - Neurotoxicity mechanisms of manganese in the central nervous system, in: M. Aschner, L.G.B.T.-A. in N. Costa (Eds.), Neurotox. Met. Old Issues New Dev., Academic Press, 2021: pp. 215–238. https://doi.org/https://doi.org/10.1016/bs.ant.2020.11.003.

[61] T.A.L. DAVIES, Manganese pneumonitis., Br. J. Ind. Med. 3 (1946) 111–135. https://doi.org/10.1136/oem.3.3.111.

[62] Y. Jiang, W. Zheng, Cardiovascular toxicities upon manganese exposure., Cardiovasc. Toxicol. 5 (2005) 345–354. https://doi.org/10.1385/ct:5:4:345.

[63] G.J. Li, L.-L. Zhang, L. Lu, P. Wu, W. Zheng, Occupational exposure to welding fume among welders: alterations of manganese, iron, zinc, copper, and lead in body fluids and the oxidative stress status., J. Occup. Environ. Med. 46 (2004) 241–248. https://doi.org/10.1097/01.jom.0000116900.49159.03.

[64] S. Alejandro, S. Höller, B. Meier, E. Peiter, Manganese in plants: from acquisition to subcellular allocation, Front. Plant Sci. 11 (2020) 517877.

[65] Y. Oulhote, D. Mergler, B. Barbeau, D.C. Bellinger, T. Bouffard, M.-È. Brodeur, D. Saint-Amour, M. Legrand, S. Sauvé, M.F. Bouchard, Neurobehavioral function in school-age children exposed to manganese in drinking water, Environ. Health Perspect. 122 (2014) 1343–1350. https://doi.org/10.1289/ehp.1307918.

[66] Bis, Indian Standard Drinking Water Specification IS 10500, Bur. Indian Stand. 25 (2012) 1–3.

[67] R.W. Herschy, Water quality for drinking: WHO guidelines, Encycl. Earth Sci. Ser. (2012) 876–883. https://doi.org/10.1007/978-1-4020-4410-6_184.

[68] M. Mainguy, C. Tognazzi, J.-M. Torrenti, F. Adenot, Modelling of leaching in pure cement paste and mortar, Cem. Concr. Res. 30 (2000) 83–90. https://doi.org/https://doi.org/10.1016/S0008-8846(99)00208-2.

[69] F. Adenot, M. Buil, Modelling of the corrosion of the cement paste by deionized water, Cem. Concr. Res. 22 (1992) 489–496. https://doi.org/https://doi.org/10.1016/0008-8846(92)90092-A.

[70] W. Zhang, D. Shi, Z. Shen, J. Zhang, W. Shao, H. Li, S. Zhao, Q. Li, R. Cao, An

approach for quantifying the calcium leaching effect on service performance of concrete cutoff wall of embankment dams, Constr. Build. Mater. 407 (2023) 133489. https://doi.org/10.1016/j.conbuildmat.2023.133489.

[71] ASTM C109/C109M– 13, Standard Test Method for Compressive Strength of Hydraulic Cement Mortars., n.d.

[72] H. Ma, Multi-scale modeling of the microstructure and transport properties of contemporary concrete, (2013).

[73] A. Hanif, P. Parthasarathy, Z. Lu, M. Sun, Z. Li, Fiber-reinforced cementitious composites incorporating glass cenospheres – Mechanical properties and microstructure, Constr. Build. Mater. 154 (2017) 529–538. https://doi.org/https://doi.org/10.1016/j.conbuildmat.2017.07.235.

[74] J.I. Bhatty, Hydration versus strength in a portland cement developed from domestic mineral wastes — a comparative study, Thermochim. Acta. 106 (1986) 93–103. https://doi.org/https://doi.org/10.1016/0040-6031(86)85120-6.

[75] A. Hanif, Z. Lu, S. Diao, X. Zeng, Z. Li, Properties investigation of fiber reinforced cement-based composites incorporating cenosphere fillers, Constr. Build. Mater. 140 (2017) 139–149. https://doi.org/10.1016/j.conbuildmat.2017.02.093.

[76] H.G. Midgley, The determination of calcium hydroxide in set Portland cements, Cem. Concr. Res. 9 (1979) 77–82. https://doi.org/https://doi.org/10.1016/0008-8846(79)90097-8.

[77] A. Hanif, P. Parthasarathy, H. Ma, T. Fan, Z. Li, Properties improvement of fly ash cenosphere modified cement pastes using nano silica, Cem. Concr. Compos. 81 (2017) 35–48. https://doi.org/10.1016/j.cemconcomp.2017.04.008.

[78] D. Londono-Zuluaga, A. Gholizadeh-Vayghan, F. Winnefeld, F. Avet, M. Ben Haha, S.A. Bernal, Ö. Cizer, M. Cyr, S. Dolenec, P. Durdzinski, J. Haufe, D. Hooton, S. Kamali-Bernard, X. Li, A.T.M. Marsh, M. Marroccoli, M. Mrak, Y. Muy, C. Patapy, M. Pedersen, S. Sabio, S. Schulze, R. Snellings, A. Telesca, A. Vollpracht, G. Ye, S. Zhang, K.L. Scrivener, Report of RILEM TC 267-TRM phase 3: validation of the R3 reactivity test across a wide range of materials, Mater. Struct. Constr. 55 (2022). https://doi.org/10.1617/s11527-022-01947-3.

[79] X. Li, R. Snellings, M. Antoni, N.M. Alderete, M. Ben Haha, S. Bishnoi, Ö. Cizer, M. Cyr, K. De Weerdt, Y. Dhandapani, J. Duchesne, J. Haufe, D. Hooton, M. Juenger, S. Kamali-Bernard, S. Kramar, M. Marroccoli, A.M. Joseph, A. Parashar, C. Patapy, J.L. Provis, S. Sabio, M. Santhanam, L. Steger, T. Sui, A. Telesca, A. Vollpracht, F. Vargas, B. Walkley, F. Winnefeld, G. Ye, M. Zajac, S. Zhang, K.L. Scrivener, Reactivity tests for supplementary cementitious materials: RILEM TC 267-TRM phase 1, Mater. Struct. Constr. 51 (2018). https://doi.org/10.1617/s11527-018-1269-x.

[80] ASTM C1897-20, Standard Test Methods for Measuring the Reactivity of Supplementary Cementitious Materials by Isothermal Calorimetry and Bound Water Measurements, ASTM Int. West Conshohocken, PA. 04 (2020) 7–11. https://doi.org/10.1520/C1897-20.2.

[81] Astm, Standard Test Method for iTeh Standards iTeh Standards Document Preview, ASTM Int. 1 (2010) 5–7. https://doi.org/10.1520/C0230.

[82] Standard Test Method, F. of H.C. Mortar, Standard, A., C1437, Astm C1437. (2009) 15–16. www.astm.org.

[83] F. Elyasigorji, F. Farajiani, M.H. Manjili, Q. Lin, S. Elyasigorji, V. Farhangi, H. Tabatabai, Comprehensive Review of Direct and Indirect Pozzolanic Reactivity Testing Methods, (2023).

[84] W. Zhang, D. Shi, Z. Shen, X. Wang, L. Gan, W. Shao, P. Tang, H. Zhang, S. Yu, Effect of calcium leaching on the fracture properties of concrete, Constr. Build. Mater. 365 (2023) 130018. https://doi.org/https://doi.org/10.1016/j.conbuildmat.2022.130018.

[85] J. Jain, N. Neithalath, Analysis of calcium leaching behavior of plain and modified cement pastes in pure water, Cem. Concr. Compos. 31 (2009) 176–185. https://doi.org/10.1016/j.cemconcomp.2009.01.003.

[86] C. Jiang, L. Jiang, X. Tang, J. Gong, H. Chu, Impact of calcium leaching on mechanical and physical behaviors of high belite cement pastes, Constr. Build. Mater. 286 (2021) 122983. https://doi.org/https://doi.org/10.1016/j.conbuildmat.2021.122983.

[87] Z. Ming, Z. Dujian, L. Tiejun, Q. Shanshan, Z. Ao, Calcium Leaching Mechanism of Cementitious Materials in the Marine Environment, J. Mater. Civ. Eng. 35 (2023) 4023122. https://doi.org/10.1061/JMCEE7.MTENG-14888.

[88] A.K. Chishi, L. Gautam, Sustainable use of silica fume in green cement concrete production: a review, Innov. Infrastruct. Solut. 8 (2023) 195. https://doi.org/10.1007/s41062-023-01164-z.

[89] M. Rafieizonooz, J.-H. Jay Kim, J. Kim, J.-B. Jo, E. Khankhaje, Microstructure, XRD, and strength performance of ultra-high-performance lightweight concrete containing artificial lightweight fine aggregate and silica fume, J. Build. Eng. 94 (2024) 109967. https://doi.org/https://doi.org/10.1016/j.jobe.2024.109967.

[90] S. Muzenski, I. Flores-Vivian, K. Sobolev, Ultra-high strength cement-based composites designed with aluminum oxide nano-fibers, Constr. Build. Mater. 220 (2019) 177–186. https://doi.org/https://doi.org/10.1016/j.conbuildmat.2019.05.175.

[91] A.M. Zeyad, B.A. Tayeh, A. Adesina, A.R.G. de Azevedo, M. Amin, M. Hadzima-Nyarko, I. Saad Agwa, Review on effect of steam curing on behavior of concrete, Clean. Mater. 3 (2022) 100042.

https://doi.org/https://doi.org/10.1016/j.clema.2022.100042.

[92] J. Hu, Z. Ge, K. Wang, Influence of cement fineness and water-to-cement ratio on mortar early-age heat of hydration and set times, Constr. Build. Mater. 50 (2014) 657–663. https://doi.org/10.1016/j.conbuildmat.2013.10.011.

[93] Z. Mo, X. Gao, A. Su, Mechanical performances and microstructures of metakaolin contained UHPC matrix under steam curing conditions, Constr. Build. Mater. 268 (2021) 121112. https://doi.org/https://doi.org/10.1016/j.conbuildmat.2020.121112.

[94] A.M. Zeyad, M.A.M. Johari, Y.R. Alharbi, A.A. Abadel, Y.H.M. Amran, B.A. Tayeh, A. Abutaleb, Influence of steam curing regimes on the properties of ultrafine POFA-based high-strength green concrete, J. Build. Eng. 38 (2021) 102204. https://doi.org/https://doi.org/10.1016/j.jobe.2021.102204.

[95] J. Zhang, T. Chen, X. Gao, Incorporation of self-ignited coal gangue in steam cured precast concrete, J. Clean. Prod. 292 (2021) 126004. https://doi.org/https://doi.org/10.1016/j.jclepro.2021.126004.

Vitae

Name : Shayiq Rashid

Nationality : India

Date of Birth : 7/6/2000

Email : shayiqrashid.sa@gmail.com

Address : Kongamdara, Pattan, Baramulla, J&K, India (193121)

Academic Background : MSc in Civil Engineering, KFUPM, KSA

B.E in Civil Engineering, VTU, INDIA

Publications

Shayiq Rashid, Hammad Raza Khalid, Asad Hanif. “Mechanical Behavior and leaching characteristics of cementitious composites incorporating silicomanganese fume”, submitted to Journal